

UNIVERSITY OF OKLAHOMA

GRADUATE COLLEGE

UNCERTAINTY ANALYSIS FOR IN-SITU FAN CURVE CALIBRATION IN  
VARIABLE AIR VOLUME SYSTEMS

A THESIS

SUBMITTED TO THE GRADUATE FACULTY

in partial fulfillment of the requirements for the

Degree of

MASTER OF SCIENCE

By

ALEJANDRO L. RIVAS PRIETO

Norman, Oklahoma

2016

UNCERTAINTY ANALYSIS FOR IN-SITU FAN CURVE CALIBRATION IN  
VARIABLE AIR VOLUME SYSTEMS

A THESIS APPROVED FOR THE  
SCHOOL OF AEROSPACE AND MECHANICAL ENGINEERING

BY

---

Dr. Li Song, Chair

---

Dr. Feng C. Lai

---

Dr. Wilson E. Merchán-Merchán



## **Acknowledgements**

First, I want to thank God for giving me peace, strength and health every morning for waking up and pursuing my goals.

Secondly, I want to thank my advisor, Dr. Li Song, for believing in me and giving me an opportunity to achieve success in my life based on hard work and dedication. I want to thank her for her constant support and lessons, which allowed me to grow as a professional in the United States. I would like to thank my research teammates Oluwaseyi Ogunsola, Jesus Elizondo and Wesley Thomas for helping me through all my adaptation process and with the diverse range of tasks that we needed to perform as part of our research group.

Thirdly, I would like to thank Daniela Arellano, my girlfriend, for being there for me, for pushing me to keep doing my best every day and pursuing my dreams. Thanks for being a breath of fresh air every time I was stressed out due to the huge amount of responsibilities that I had to face after leaving my beloved country, Venezuela.

Last, I want to thank my family, friends and Venezuela for reminding me every day who I am and where I come from. My achievements are also yours, because all of you are part of who I am today. Because of this and many more reasons, GRACIAS.

# Table of Contents

Acknowledgements .....	iv
List of Tables .....	viii
List of Figures.....	ix
Abstract.....	xi
Chapter 1: Introduction .....	1
1.1. HVAC and VAV AHU Overview .....	1
1.2. Airflow Measurement Overview .....	4
1.3. Virtual Airflow Meters .....	8
1.4. Challenges in in-situ Airflow Measurements for Calibration of VAV AHU ..	10
1.5. Objectives of the Thesis.....	12
Chapter 2: Measurement Equipment and Test Set-Up.....	16
2.1 Fan Performance Curves.....	16
2.2 Test Air Handling Units.....	20
2.3 Measurement Equipment .....	22
2.3.1 Fan power, speed, and head measurements.....	22
2.3.2 Airflow velocity measurement .....	22
2.3.3 Holding bracket prototype .....	23
2.3.4 Data acquisition devices .....	25
2.4 Test Set-Up .....	26
Chapter 3: Temporary Airflow Measurements for an Extended Time .....	28
3.1. Sampling Time.....	29
3.1.1 AHU-5 .....	31

3.1.2	AHU-6 .....	33
3.1.3	AHU-9 .....	34
3.1.4	Summary.....	37
3.2	Sampling Points .....	39
3.2.1	AHU-5 .....	42
3.2.2	AHU-6 .....	43
3.2.3	AHU-9 .....	44
3.2.4	Summary.....	45
3.3	Location Factor .....	46
3.4	Industry Standard Thermal Sensor Measurements .....	49
3.4.1	AHU-5 .....	51
3.4.2	AHU-6 .....	52
3.4.3	AHU-9 .....	53
3.4.4	Summary.....	54
Chapter 4:	In-situ Fan Curve Calibration of VAV AHU .....	56
4.1	Calibration Procedure .....	57
4.2	Uncertainty Analysis.....	58
4.2.1	Uncertainty and error for input variables .....	58
4.2.2	Error propagation.....	60
4.3	Fan Performance Curves.....	65
4.3.1	AHU-5 .....	65
4.3.2	AHU-9 .....	66
4.3.3	Summary.....	68

Chapter 5: Conclusions and Future Work .....	69
References .....	72
Appendix A: Abbreviations.....	76
Appendix B: AFMS Industry Guidelines .....	78

## List of Tables

Table 2-1: Basic design information of selected VAV AHUs .....	20
Table 2-2: Actual duct lengths vs. required duct lengths .....	21
Table 3-1: Reduced number of sampling points analysis for SA AHU-5 .....	42
Table 3-2: Reduced number of sampling points analysis for RA AHU-5 .....	42
Table 3-3: Reduced number of sampling points analysis for SA AHU-6.....	43
Table 3-4: Reduced number of sampling points analysis for RA AHU-6 .....	43
Table 3-5: Reduced number of sampling points analysis for SA AHU-9.....	44
Table 3-6: Reduced number of sampling points analysis for RA AHU-9 .....	44
Table 3-7: Summary of RMSE and RMSE% .....	45
Table 3-8: Percentages of compensated straight duct lengths .....	46



## List of Figures

Figure 1-1: VAV system schematic .....	3
Figure 1-2: Common HVAC airflow measurement devices .....	5
Figure 1-3: Typical velocity pressure distributions.....	6
Figure 1-4: Traverse locations by Equal-Area and log-T methods .....	11
Figure 2-1: Typical fan performance curves .....	16
Figure 2-2: Method of obtaining fan performance curves.....	17
Figure 2-3: Variable-speed fan in a VAV system .....	18
Figure 2-4: Selected VAV AHUs' basic schematic .....	20
Figure 2-5: Layout and dimensions of testing stations.....	21
Figure 2-6: VFD for RF and DP sensor installed across the SF.....	22
Figure 2-7: Typical placement of holes for TAB procedures.....	23
Figure 2-8: Designed and manufactured holding bracket .....	24
Figure 2-9: Hot-wire velocity probe mounting in AHU-6 for performing traverse measurements .....	24
Figure 2-10: Utilized DAQ for recording airflow measurements .....	25
Figure 2-11: Testing set-up for performing in-situ airflow measurements .....	26
Figure 3-1: Traverse grid for SA and RA sections in AHU-6.....	30
Figure 3-2: Average velocity vs. sampling time by traverse and 3-P for SA AHU-5....	31
Figure 3-3: Average velocity vs. sampling time by traverse and 3-P for RA AHU-5 ...	32
Figure 3-4: Average velocity vs. sampling time by traverse and 3-P for SA AHU-6....	33
Figure 3-5: Average velocity vs. sampling time by traverse and 3-P for RA AHU-6 ...	34
Figure 3-6: Average velocity vs. sampling time by traverse and 3-P for SA AHU-9....	35

Figure 3-7: Average velocity vs. sampling time by traverse and 3-P for RA AHU-9 ...	35
Figure 3-8: Average velocity by traverse for SA at 1480 fpm and RA at 975 fpm during testing .....	36
Figure 3-9: Average velocity vs. sampling time from the 70th second by traverse and 3-P for SA AHU-9 .....	37
Figure 3-10: Comparisons of 3-P vs. traverse relative differences for SA and RA measurements .....	38
Figure 3-11: Normalized velocity for SA and RA in AHU-6 .....	47
Figure 3-12: Combined RMSEk vs. location factor .....	49
Figure 3-13: AFMS sampling point locations for SA and RA of AHU-6.....	50
Figure 3-14: SA and RA by 3-P and AFMS comparison to traverse for AHU-5 .....	51
Figure 3-15: SA and RA by 3-P and AFMS comparison to traverse for AHU-6 .....	52
Figure 3-16: SA and RA by 3-P and AFMS comparison to traverse for AHU-9 .....	53
Figure 3-17: Linear fitting residuals for 3-P and AFMS compared to traverse measurements .....	54
Figure 4-1: Laboratory testing requirements for the outlet and inlet of fans .....	56
Figure 4-2: Fan performance curves for SF AHU-5 .....	65
Figure 4-3: Fan performance curves for RF AHU-5.....	65
Figure 4-4: Fan performance curves for SF AHU-9 .....	67
Figure 4-5: Fan performance curves for RF AHU-9.....	67

## **Abstract**

In order to obtain in-situ fan performance curves for variable air volume (VAV) air handling units (AHUs) with predicted uncertainties, airflow measurements for an extended time and a tailored calibration procedure were proposed and validated in this work.

To obtain airflow measurement for an extended time, traverse measurements through the Equal-Area method were first conducted to select 3 sampling points (3-P) that represented the average velocity at a measurement plane. Next, through statistical analysis, additional uncertainty generated when reducing the number of sampling points was accounted for in terms of sampling time, reduced number of sampling points, measurement location, and comparison to common airflow measurement stations (AFMS). As a result of these analyses, it was found that for sampling times of 60 seconds, uncertainties below 5% can be expected from 3-P measurements when airflow velocity is above 800 fpm. Analysis showed that for return air (RA) measurements where velocities below 800 fpm are common, more than 3-P would be necessary to comply with 5% accuracy per ASHRAE Standard 111 [2008] requirements.

Next, it was demonstrated through comparison of measurement conditions and uncertainties for supply air (SA) that a relationship between measurement location and uncertainty of the 3-P measurement exists. Finally, the results showed that AFMS utilized more sampling points than necessary to achieve 5% accuracy in every test case. Performing airflow measurements with a tailored selection of sampling points was more effective than following cross-sectional area-based industry guidelines.

Upon the completion of the airflow uncertainty analyses, a calibration procedure for VAV AHUs was also produced and tested to obtain in-situ fan performance curves. In addition, based on the ANSI/ASHRAE Standard 51 [1999], an uncertainty analysis was performed on adjusted measurements by fan laws to build in-situ fan performance curves. Uncertainty bands at 95% confidence showed that previously defined airflow measurement uncertainty is the most sensible variable. Results showed that while application of fan laws can be applicable to return fans (RFs), higher uncertainties can be expected as airflow velocities below 800 fpm are common. Nevertheless, since SA average velocities were generally above 800 fpm, narrow uncertainty intervals were observed.

In conclusion, a practical and reliable approach for in-situ fan performance curves calibration was explored using statistical analysis and uncertainty propagation of airflow, fan head, and fan power uncertainties. Airflow measurements for extended sampling times were successfully achieved after developing a prototype holding bracket design for reducing field technician dependency. Finally, a VAV AHU calibration procedure for obtaining in-situ fan performance curves with actual range and visible system effect impacts was successfully applied and validated through this thesis work.

# **Chapter 1: Introduction**

## **1.1. HVAC and VAV AHU Overview**

Heating, Ventilating and Air Conditioning (HVAC) systems are the most common systems for indoor environment control. They provide occupants in enclosed spaces with satisfactory conditions to support their daily activities in healthy and comfortable environments by controlling temperature, humidity, contaminants, and other factors. To achieve this goal, HVAC systems have been constantly evolving from the caveman's simple desire of finding shelter for protection from weather conditions to 21<sup>st</sup> century complex requirements for every human indoor activity.

According to Branesky [2013], the technology for indoor climatization began in the 1890s. World War II gave a push to the technology in locations like Houston and Dallas, which were considered to be the most air-conditioned cities in North America by the 1950s and early 1960s [Int-Hout, 2015]. In the 1960s, contractors in Dallas started to apply new types of systems with high velocity induction reheat, airside economizers and variable air volume (VAV) units that were more flexible for conditioning multiple spaces or zones within a building [Int-Hout, 2015].

In 1974, with the worldwide increase of oil prices, the HVAC industry needed to be more energy conscious regarding fuel's utilization [Int-Hout, 2015]. This situation was the basis for the wide implementation of VAV systems as a solution for achieving building energy efficiency in the United States.

The constant air volume (CAV) system has been widely used ever since the invention of climatization technology. This type of air handling unit (AHU) supplies a constant

amount of conditioned air (regardless of changes in the dynamic building thermal load). Therefore, in CAV systems, the space temperature can be varied by re-heating the supplied air to avoid overcooling of the space. Consequently, significant energy waste exists due to simultaneous cooling and heating. Instead, VAV systems vary the amount of conditioned supply air to control the space's temperature according to fluctuations in building load. The supply airflow (SA) in a VAV system is usually modulated with the implementation of variable frequency or speed drives (VFD or VSD) that control a motor connected to a fan(s) in an AHU. Since individual space temperature can be maintained by implementing VAV systems without the need of re-heating, greater energy savings and constant comfort conditions can be accomplished on a regular basis [ASHRAE, 2016].

However, in addition to the advantages that VAV systems have in comparison to CAV systems, there are many challenges for achieving their full potential in energy savings. Each of these challenges requires research and development to make the VAV system perform in the way that it was intended with its development.

Figure 1-1 presents a typical schematic of a VAV system. In this schematic, we can identify the Supply Fan (SF), which provides the fan head necessary for distributing the conditioned air to each zone. This SF operates with a VFD to vary its speed according to the instantaneous cooling/heating load. Air is cooled/pre-heated by a heat exchanger or cooling/heating coil. The air needs to be filtered to ensure that the supplied air will be free of hard particles. The SA is composed of a mixture of returned air from spaces and outdoor air. With this approach, energy consumption can be reduced and indoor air quality (IAQ) is ensured to maintain healthy conditions for occupants. The mixture of

these two air sources is done by a Mixing Air Plenum and Dampers that can regulate a fraction of the mixture. Since a building cannot be over-pressurized by the addition of outdoor air (OA), some air needs to be relieved from the return air (RA) during an economizer when more mild OA is introduced for utilizing free cooling. This task is performed by the Return/Relief Air Plenum and a Relief Air Damper. An arrangement of pressure sensors will control the relief damper to release the right amount of air. Moreover, when an economizer is adopted, a VAV system needs to have a Return Fan (RF) to release the air. When a RF is required in a VAV system, it will have a separate VFD for controlling the amount of RA according to pressure from the outdoors and the return/relief air plenum. In this way, the RF reacts to the SF instantaneous speed and ensures that the correct amount of air is being returned and building pressurization is maintained, as required by building codes.

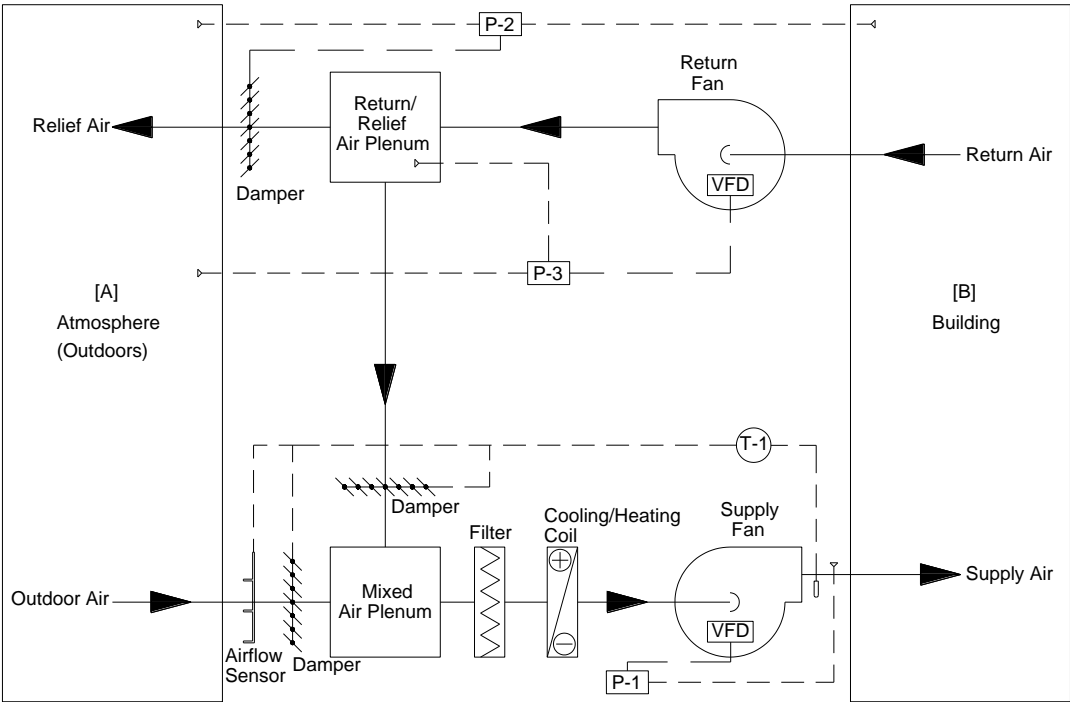


Figure 1-1: VAV system schematic (Source: ASHRAE, 2003).

The VAV system's real-time control of the heating and cooling loads makes airflow rate measurements critical in the system operation for the following reasons:

1. To ensure IAQ: ASHRAE 62.1 [2013c] indicates that a minimum amount of outdoor air needs to be maintained in every system (especially VAV systems) through the constant control of dampers and/or fans. To achieve this goal, permanent airflow rate sensors are commonly installed for providing required feedback and reducing response time of the system.
2. To calibrate the VAV AHU: airflow measurements are needed during the commissioning phase for ensuring that the HVAC system is delivered in hands of the building's owner and operates at the design capacity.
3. To calibrate permanent sensors: in-situ airflow measurements allow for identification and correction of any bias errors or inconsistency in airflow readings obtained from installed permanent sensors in the VAV system.

## **1.2. Airflow Measurement Overview**

Airflow measurement is essential for characterizing the operation and performance of air conditioning equipment. In VAV systems, airflow measurements are becoming increasingly important for reliable energy efficient operations. However, airflow measurements in VAV systems are challenging for two reasons [Rivas Prieto et al., 2016b]:

1. Long straight ductwork for accurate flow measurements of traditional airflow sensors is usually not available in most mechanical rooms.







2. Traditional airflow sensors, such as Pitot-static tubes, Orifice plates, or Venturi meters, work well at high airflow rates (i.e., high air velocity), but the accuracy losses are significant at low flow rates, which VAV AHUs often run into with dynamic load changes.

In the HVAC industry, airflow measurements are usually carried out by the following two types of devices [Damiano ,2012]:

1. Differential Pressure airflow sensors
2. Thermal Velocity airflow sensors

They can be permanently installed or used as a hand-held (portable) device [Damiano, 2012], depending on different applications and objectives of the airflow measurement.

Figure 1-2 shows some of the most typical airflow measurement devices used in HVAC systems.

Type of Device	Differential Pressure	Thermal Velocity
Hand-Held		
Permanent		

**Figure 1-2: Common HVAC airflow measurement devices (Source: Damiano, 2012).**

Permanent flow measurement devices in ducts mainly include differential pressure sensors such as Pitot-static tube arrays and thermal velocity sensors. The differential pressure sensor arrays average the static pressure and total pressure measurements from all the measurement nodes and then calculate the average velocity. Due to the nonlinearity between the velocity and differential pressure, one study found an 11% measurement error that was solely caused by non-linear averaging [Damiano, 2012]. Thermal velocity sensors consist of a number of single-point sensors arranged in a traverse-like pattern or array. The single-point velocity measurements are averaged together to yield an output signal that is representative of the average duct flow. Moreover, thermal velocity sensors are favored in permanent installations because of their consistent accuracy under lower velocities such as 600 fpm [Rivas Prieto et al., 2016a].

Permanently-installed airflow sensors in ducts require a distance of 7.5 hydraulic diameters downstream and 3 hydraulic diameters upstream from a disturbance (e.g., a fitting) in order to obtain well developed velocity distribution for the flow measurements [ASHRAE, 2013a]. Besides these length requirements, ASHRAE Standard 111 [2008] indicates that a well-developed velocity distribution for accurate airflow measurement is identified when 80% to 90% of the airflow measurements' velocities are above the value of 10% of the maximum measured velocity on a measurement plane (see Figure 1-3).

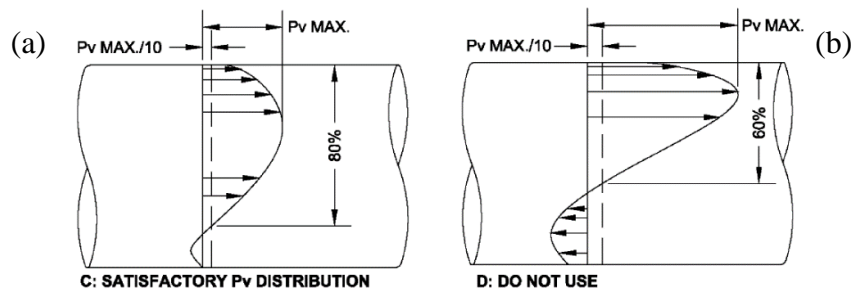


Figure 1-3: Typical velocity pressure distributions (Source: ASHRAE, 2008).

In contrast, due to limited space available in mechanical rooms, the length requirements for obtaining well-developed velocity profiles are usually not available in practice. Therefore, steady and symmetric velocity distributions are usually not available on a measurement plane. A study presented by Damiano [2012] reported up to 43.2% errors for Pitot-tube arrays when choosing measurement locations not in agreement with ideal length requirements to and from disturbances.

In contrast to permanent devices, hand-held flow measurement devices are intended to be used by technicians for TAB systems as outlined by ASHRAE Standard 111 [2008] and Chapter 38 of the ASHRAE Applications Handbook [2015]. The main goal of these devices is to calibrate installed permanent devices while considering in-situ or field conditions. Nonetheless, accuracy of these devices is greatly dependent on technicians' skills and the device type itself. Some factors that impact the airflow's velocity measurement accuracy are:

- Technician's experience
- Well-developed velocity profile
- Low velocity (airflow velocity below 10 fpm)
- Number of sampling points in the cross-sectional area of the air ductwork
- Direction of the airflow in relation to the measurement device's sensing point

To ensure accuracy of in-situ airflow measurements, standard procedures have been developed to provide guidance on the selection and implementation of measurement devices. According to ASHRAE Standard 111 [2008], in typical HVAC applications where airflow velocity will be encountered between 10 fpm and 600 fpm, the standard

suggests thermal velocity measurement devices. For higher velocities, the Pitot-static tube can represent a good alternative. It is also outlined that the rotation of the device axis should not exceed  $\pm 20^\circ$  from the perpendicular to the flow direction.

Moreover, ASHRAE Standard 111 [2008] indicates how the measurement location (traverse plane) should be selected and the minimum number/position of sampling points that are needed, according to methods such as log-Tchebycheff (log-T) rule or Equal Area for obtaining a representative and accurate value of the average airflow's velocity. However, since ideal conditions are not commonly met in the field, the standard suggests maximizing the number of sampling points if needed, which is one of the major factors impacting the uncertainty of airflow measurements.

Therefore, when dealing with VAV systems in which the permanent measurement of airflow is required for ensuring appropriate control of the VAV AHU, the uncertainty in airflow measurements performed during TAB procedures will have a lasting effect on the performance of the overall equipment and associated energy consumption of the HVAC system. Moreover, when the uncertainty of airflow measurement increases, there can be a poor feedback input to the control system that can lead to issues such as 15% to 30% additional energy consumption [Wang et al., 2014], IAQ issues, overcooling or overheating effects that will affect comfort conditions, etc.

### **1.3. Virtual Airflow Meters**

Due to the increasing need for more accurate ways of measuring airflow in VAV systems, some technologies have been developed to calculate airflow while eliminating the need for physical installation of airflow sensors. By performing this indirect measurement

approach, some sources of uncertainty can be dismissed from the airflow measurements. One of these indirect methods is the concept of a Virtual Airflow Meter (VAFM). Since fan performance curves relate actual fan airflow rate to other measurable operational variables such as fan head, speed, and shaft power, the airflow rate through a fan can theoretically be determined based on these variables using fan performance curves [Rivas Prieto et al., 2016b]. Much research has been conducted on a fan's virtual flow sensors. Liu [2002] proposed a head-based fan airflow sensor, which determines the airflow rate based on the measured fan speed and head using an in-situ fan head curve. Experiments were conducted in a full-size AHU in a laboratory [Yuill et al., 2003]. The directly measured airflow rate showed excellent agreement with the airflow rate calculated by a fan airflow sensor in laboratory testing. Head-based fan airflow sensors were also implemented in a number of AHUs for building pressure control [Liu et al., 2005]. As a complementary improvement, a power-based fan airflow sensor was developed by Wang and Liu [2007]. The power-based fan airflow sensor determines the fan airflow using measured motor power rather than fan head associated with an in-situ fan power curve. Moreover, Wang and Liu [2005] developed a power head-based fan airflow sensor. Fan airflow is determined based on the measured fan head and motor power using a calibrated fan efficiency curve.

In general, the studied virtual fan airflow sensors calculate the airflow rate based on other measurable operational variables, such as fan head, fan speed, and motor power using in-situ fan performance curves, i.e., fan head, motor power, or fan efficiency curves. The calibration of in-situ fan curves is critical for the successful implementation of virtual airflow sensors. Manufacturers' fan curves are usually not applicable due to actual fan

installation configuration and actual location of the differential pressure sensor for fan head measurement [Liu et al., 2005]. Therefore, an accurate in-situ fan curve is necessary to develop a virtual fan airflow sensor. Flow measurements present a major challenge to calibrating in-situ fan curves [Rivas Prieto et al., 2016b].

#### **1.4. Challenges in in-situ Airflow Measurements for Calibration of VAV AHU**

An extended period of in-situ flow measurements is needed in order to cover different fan operation scenarios under a wide range of operations and obtain accurate and robust in-situ fan curves [Rivas Prieto et al., 2016b]. The extended period of in-situ flow measurements provides unique challenges:

1. Hand-held devices will no longer be effective.
2. Traditional methods like log-T and Equal Area (see Figure 1-4) will present practical issues since the high sampling point density is not feasible for extended period measurements.

Therefore, there is a need to reduce the number of sampling points for making the procedure suitable for in-situ conditions in VAV systems. Research has been done to verify the measurement accuracy when using fewer measurement points than required by the common traverse methods [Rivas Prieto et al., 2016a]. Through laboratory testing, Schwenk [1998] concluded that 3-point airflow measurements could provide accuracy comparable to a 35-point traverse measurement. The Damiano [2012] study concluded that 6 thermal dispersion probe measurements worked much better than 14-point differential pressure sensor measurements.

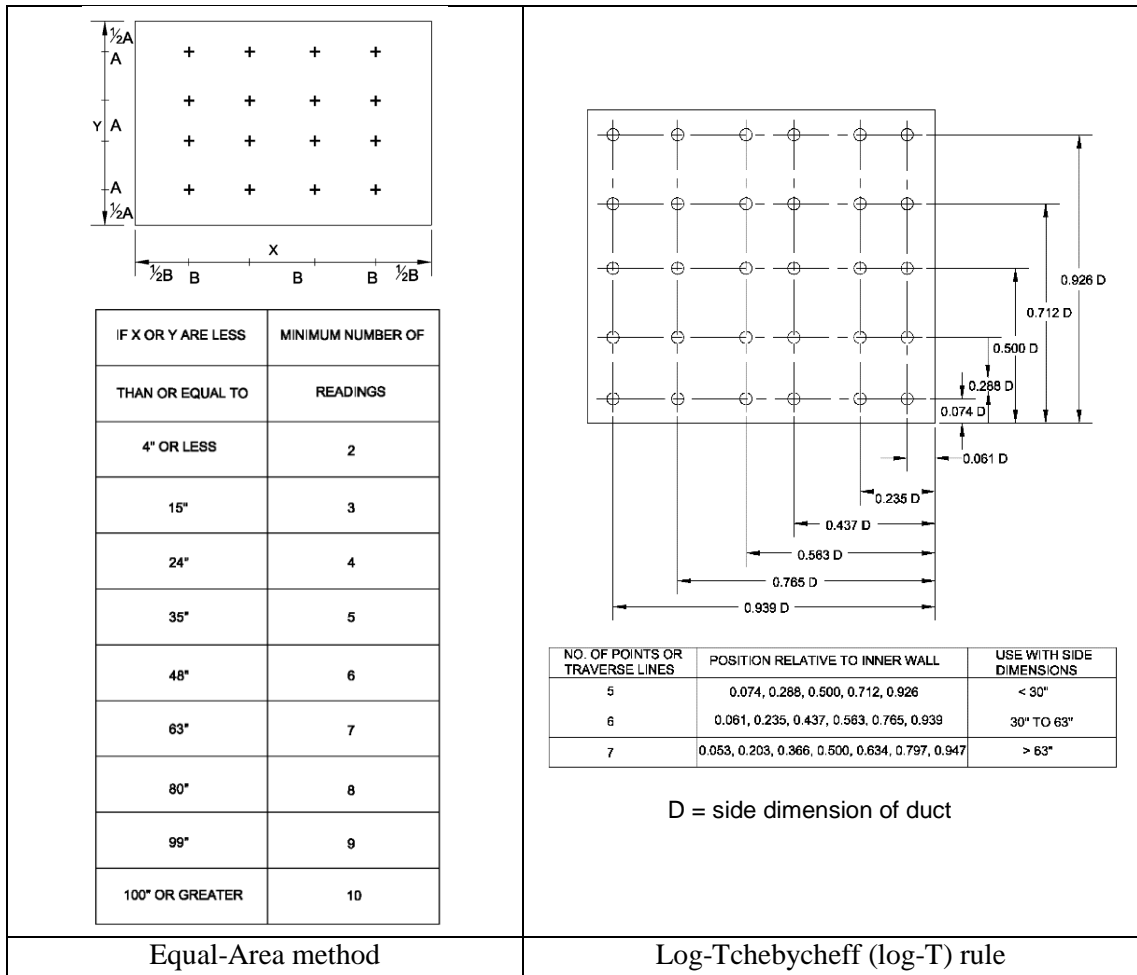


Figure 1-4: Traverse locations by Equal-Area and log-T methods (Source: ASHRAE, 2008).

Rivas Prieto et al. [2016a] found that lower measurement density can significantly reduce measurement costs, especially for thermal velocity sensors which average single-point velocities. However, fewer measurement points will not have full coverage of the velocity distribution in ducts and will potentially lead to significant bias of the flow rate measurements if the selected points are not representative of the mean velocity in ducts. As a result, a manual traverse might be a solution to identify the representative measurement points by comparing the results using one-time traverse measurements under the same flow conditions. However, when flow rates change, the selected representative measurement points may no longer be representative of the mean velocity

calculations if the velocity distribution on a cross-sectional plane does not change similarly as the total airflow rate changes in the ducts, i.e., the velocity distribution profile does not experience homothetic changes as flowrate changes in ducts. The non-homothetic velocity distribution changes will introduce additional uncertainty to the mean velocity calculations when an insufficient number of measurement points are used. The non-homothetic changes of the velocity distribution are related to a fluid field that is described primarily by velocity and distance to a fitting.

Airflow in the duct is generally turbulent, involving random perturbations or fluctuations of the flow. As a result, in addition to the number of sampling points, the measured velocity should be the time-averaged velocity [ASHRAE, 2013a], and consequently velocity measurements are influenced by sampling time as well.

The goal of this thesis work is to investigate the impacts of the number of sampling points and the duration of the sampling time on the measurement accuracy in order to attain a feasible in-situ fan curve measurement method that provides acceptable accuracy or quantifiable uncertainty propagated comprehensively from sensor uncertainties and the uncertainties caused by a reduced number of sampling points.

### **1.5. Objectives of the Thesis**

Three objectives will be obtained in this thesis in order to achieve the goal discussed in Section 1.4:

*Objective 1: to take temporary in-situ airflow measurements for an extended sampling time.*



In order to validate the implementation of reduced number of sampling points under non-ideal measurement conditions while increasing sampling time, Objective 1 will involve the evaluation and validation of: (1) extended sampling times for airflow velocity measurements; (2) a reduced number of sampling points compared with ASHRAE Standard 111 [2008] and the ASHRAE Fundamentals Handbook [2013a] requirements, and (3) the effect of non-ideal measurement conditions on airflow velocity measurement accuracy.

*Objective 1.1: to validate the impacts of sampling time*

ASHRAE Standard 111 [2008] and the ASHRAE Fundamentals Handbook [2013a] provide the principal guidelines for airflow measurement in the HVAC field. However, the time sampling approach for non-stable airflows provided by the standard is short and general, since it has been applied in CAV applications with ideal duct length conditions. It is important to define a time sampling interval suitable for VAV systems and its relation to measurement uncertainty.

*Proposed approach to accomplish Objective 1.1:* different sampling time averages will be applied on airflow measurement data. Then, it will be possible to analyze and compare results from different VAV AHUs to define a common measurement sampling time.

*Objective 1.2: to evaluate the accuracy of a reduced number of sampling points*

Traverse airflow measurements methods like log-T and Equal Area are suggested by ASHRAE Standard 111 [2008] and the ASHRAE Fundamentals Handbook [2013a] for TAB procedures on HVAC systems. These industry methods are based on a high density of sampling points for satisfactory accuracy. The requirement for a large number of

sampling points is possible for a hand-held device for one-time set of measurements, but is less practical for extended period airflow measurements. Therefore, it is fundamental to define uncertainty estimations associated with airflow measurements through a reduced number of sampling points.

*Proposed approach to accomplish Objective 1.2:* a reduced number of sampling points can provide a practical solution for in-situ airflow measurements if these points provide an accurate and precise airflow reading. For testing this idea, the measurement results of a different number of sampling points will be compared to suggested standard methods. Consequently, it will be possible to verify and quantify the overall uncertainty that is introduced when the number of sampling points is reduced. Additionally, the number of sampling points and locations on the measurement plane commonly applied in the field will be suggested. Then, it is possible to check the commonly introduced uncertainty by industry's standard airflow measurement points and compare it with results from the proposed measurement method.

*Objective 1.3: to evaluate the effect of non-ideal measurement conditions*

ASHRAE Standard 111 [2008] and the ASHRAE Fundamentals Handbook [2013a] describe the ideal measurement set-up for obtaining reported uncertainties from different airflow measurement methods. These conditions assume that the airflow measurement locations are 7.5 and 3 hydraulic diameters downstream and upstream, respectively, from the closest disturbance [ASHRAE, 2013a]. Nevertheless, these conditions are not usually encountered in-situ. Thus, the impact of non-ideal conditions on the accuracy of current and proposed measurement methods needs to be reviewed and compared.

*Proposed approach to accomplish Objective 1.3:* the impact of non-ideal airflow measurement conditions on airflow measurement accuracy can be analyzed by comparing different VAV AHUs with a wide range of lengths to and from disturbances in ductworks. For simplifying this task, root mean square errors (RMSE%) and uncertainties are calculated for allowing a fair comparison between study cases.

*Objective 2: to obtain in-situ fan performance curves with predicted uncertainty*

The ASHRAE HVAC Systems and Equipment Handbook [2016] outlines basic methods for defining fan performance curves. In this standard, it is indicated that additional considerations need to be implemented when the installed fan is operating under conditions significantly different than standard laboratory testing conditions. Therefore, in-situ field fan performance curve measurements are necessary. The fact that the fan operations are limited by physical and load conditions limits prohibits a wide fan operation range measurement.

*Proposed approach to accomplish Objective 2:* a step-by-step calibration procedure needs to be developed to obtain in-situ fan head and efficiency curves for both supply and return air fans that cover the majority of the operation scenarios. Additionally, these fan performance curves will include an uncertainty range that will be found through the propagation of uncertainties from airflow measurements, pressure sensors, and VFD panel power readings.

## Chapter 2: Measurement Equipment and Test Set-Up

This chapter will introduce test AHUs and the measurement apparatus in order to accomplish the objectives presented in Section 1.5. First, in Section 2.1, the theoretical background about fan head and efficiency curves will be introduced in order to determine measurement variables. In Section 2.2, test VAV AHUs will be presented along with their basic technical specifications. In Section 2.3, measurement equipment utilized for achieving extended sampling time measurements will be described. Finally, in Section 2.4, general testing set-up conditions for this thesis will be described.

### 2.1 Fan Performance Curves

Fan performance curves are usually displayed as fan head (total pressure) and fan efficiency curves versus airflow rate, as shown in Figure 2-1.

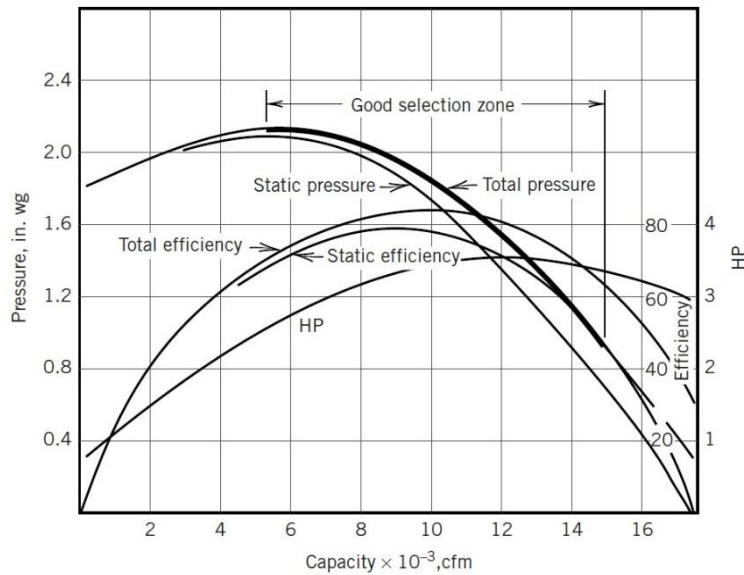


Figure 2-1: Typical fan performance curves (Source: McQuiston et al., 2005).

The fan head curve is built from the measured airflow rate and differential pressure across the fan. The fan efficiency curve is based on measured airflow and calculated efficiency (see Equation 2-1).

$$(2-1) \quad \eta = \frac{H(in.wg) \cdot Q(cf\ m)}{8507 \cdot W(kW)}$$

where  $H$  refers to fan head at 100% fan speed,  $Q$  refers to airflow at 100% fan speed, and  $W$  refers to fan power at 100% speed.

Fan curves are usually given by fan manufacturers, but the performance of an installed fan in any HVAC system always differs from the performance obtained during laboratory testing. Therefore, in-situ fan performance curves are necessary for accurate virtual fan airflow rate calculations.

Figure 2-2 illustrates the basic method for obtaining a full-range fan performance curve. When the resistance in the fan is increased (close to “blocked off” condition), the fan head increases while the airflow decreases. The testing will consist of gradually decreasing the resistance by opening dampers for increasing airflow rate until they reach a “wide open” condition.

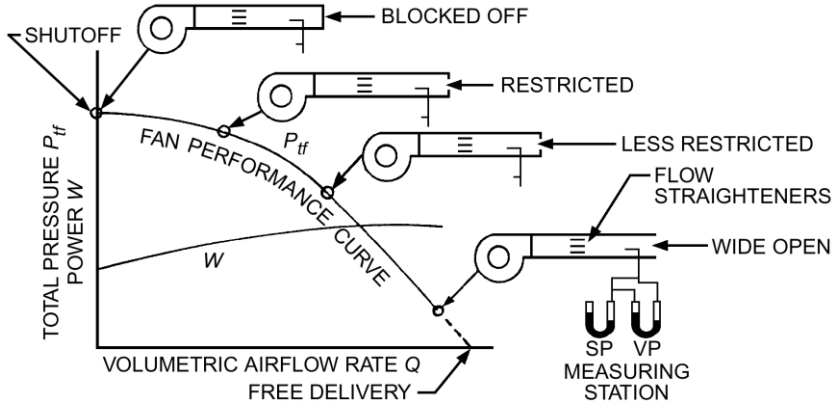


Figure 2-2: Method of obtaining fan performance curves (Source: ASHRAE, 2016).

In a VAV system, the variation of speed and dynamics generates different performance curves for fans depending on different speeds. Inevitably, the fan head and airflow rate measurements at partial speeds need to be first converted to a design speed (100%) to account for the correct definition of fan performance curves. To perform this conversion, the fan laws described in Equations 2-2 and 2-3 are applied to convert fan head and airflow rate at partial speeds to 100% (full) speed, i.e., 60 Hz.

$$(2-2) \quad H_e = \frac{H_i}{\bar{\omega}^2}$$

where  $H_e$  refers to equivalent fan head at full fan speed (100%),  $H_i$  refers to fan head at partial fan speed, and  $\bar{\omega}$  refers to the ratio of the partial speed (%) to the full speed, shown in Figure 2-3.

$$(2-3) \quad Q_e = \frac{Q_i}{\bar{\omega}}$$

where  $Q_e$  refers to equivalent airflow at full fan speed and  $Q_i$  refers to the airflow at partial speed.

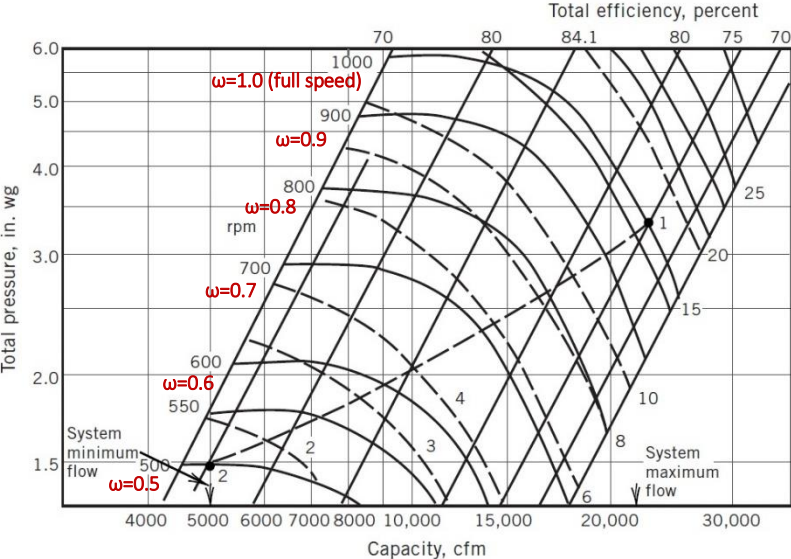


Figure 2-3: Variable-speed fan in a VAV system (Source: McQuiston et al., 2005).

In addition, according to fan laws, each point on the fan performance curve at full speed has multiple equivalent points, which have the same ratio of the fan head to the square of the airflow. Consequently, to generate a full range of the fan curve, fan operations at different ratios of the fan head to the square of the airflow need to be captured. The typical approach for changing this ratio is to adjust the system resistance by opening and closing the dampers (see Figure 2-2), such as a return air damper or terminal box dampers in an operating AHU. However, due to different damper characteristics and slow response times of the damper actuators, it is difficult to use the damper positions to make quick adjustments. Therefore, for test AHUs included in this thesis, since both the supply and return air fans are installed, different ratios of fan head to the square of airflow for the supply and return air ducts can be obtained by overriding the supply and return air fan speed with different combinations.

As a result, to generate in-situ fan performance curves (head and efficiency curves), fan head, motor input power, and airflow rate and fan speed are needed measurements. Fan head and motor input power are commonly measured in the field with robust and reliable permanent instruments like differential pressure transducers and VFD panels. Airflow rate is the third required variable to measure in order to calculate efficiency. However, this task has been identified by ASHRAE [2016] as the most sensible variable to errors when performing in-situ performance testing of fans. As previously mentioned, it is not common to find ideal measurement locations in the field for traverse airflow measurements.

## 2.2 Test Air Handling Units

The proposed experiments are to be conducted using three test VAV AHUs in a medical facility on a military base. The test AHUs have the same configuration as shown in Figure 2-4. They have both an SF and a RF, and both fans are equipped with VFDs. An outdoor air duct introduces OA to the AHU for IAQ control.

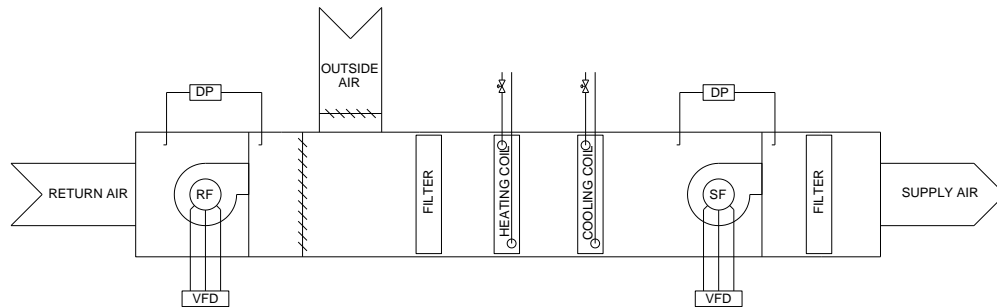


**Figure 2-4: Selected VAV AHUs' basic schematic (Source: Rivas Prieto et al., 2016a).**

The design fan airflow information for all AHUs is given in Table 2-1. Since the testing was conducted using the main ducts in the AHUs, the design velocity was calculated by the design fan airflow rate and main duct sizes while factoring in 15% system effect losses [Yong et al., 2008]. The velocity variation range for each fan in each VAV AHU is given in Table 2-1 by applying ASHRAE's recommended 30% minimum airflow rates [ASHRAE, 2013b].

**Table 2-1: Basic design information of selected VAV AHUs (Source: Rivas Prieto et al., 2016a).**

AHU	SF					RF					Cooling capacity (Btu/h)
	Airflow (cfm)		Airflow Velocity (fpm)	Airflow (cfm)		Airflow Velocity (fpm)	Airflow (cfm)		Cooling capacity (Btu/h)		
	min	max		Min	max		min	max			
5	5595	9885	11.19	538	1795	3675	7965	3.73	162	1274	396000
6	8645	11250	11.19	545	1815	4415	7020	3.73	163	1123	506000
9	5160	9735	11.19	551	1836	3210	7785	3.73	165	1135	399000



The Testing stations (TS in Figure 2-5) were located by TAB technicians when the systems were constructed. None of the TS locations comply with the ASHRAE standard due to limited space available in the mechanical rooms [ASHRAE, 2013a]. However, the TAB was conducted anyway, as it is common industry practice.

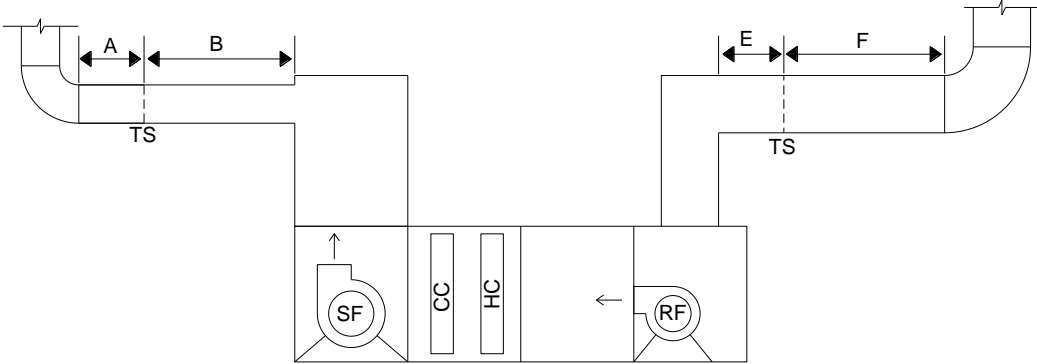


**Figure 2-5: Layout and dimensions of testing stations (Source: Rivas Prieto et al., 2016a).**

Table 2-2 summarizes the actual dimensions for each test AHU. The required straight duct lengths, according to the ASHRAE standard, were also calculated and compared with actual dimensions as shown in Table 2-2. As can be seen, none of the testing stations are satisfactory according to the ASHRAE standard. Since the dimensions in the SA ducts are all different for the three test AHUs, the SA velocities can be used to investigate the impact of non-ideal measurement conditions.

**Table 2-2: Actual duct lengths vs. required duct lengths (Source: Rivas Prieto et al., 2016a).**  
 (Note: subscript-req: required length by ASHRAE; A, B, E, F are the names of the ducts listed in Figure 2-5)

AHU	SA				RA			
	A (ft.)	B (ft.)	A <sub>req</sub> (ft.)	B <sub>req</sub> (ft.)	E (ft.)	F (ft.)	E <sub>req</sub> (ft.)	F <sub>req</sub> (ft.)
5	1.25	1.70	6.82	17.05	1.33	3.17	7.50	18.75
6	6.17	8.08	6.74	16.85	0.83	4.08	7.50	18.75
9	5.50	12.83	6.11	15.27	0.25	1.42	7.72	19.30

## 2.3 Measurement Equipment

In order to define in-situ fan performance curves, the airflow rate, fan head, fan motor input power and fan speed need to be measured and recorded for a variety of different fan speed combinations as explained in Section 2.1.

### 2.3.1 Fan power, speed, and head measurements

Figure 2-6 (a) shows the VFD of the SF, which provides fan motor input power and VFD frequency through its two 4-20mA analog outputs connected to the BAS. The VFD frequency is considered to be proportional to the fan speed. Figure 2-6 (b) shows the differential pressure (DP) sensor across the SF, which measures the fan head.



Figure 2-6: VFD for RF and DP sensor installed across the SF.

### 2.3.2 Airflow velocity measurement

The ductwork of the test AHUs has holes for air velocity probe insertion in supply and return air sides, as shown in Figure 2-7. Those holes were identified and drilled by TAB technicians according to the Equal Area method (see Figure 1-4) described in ASHRAE Standard 111 [2008]. However, due to space limitations in the mechanical room, the TS

locations do not comply with this standard. As a result, inadequate ductwork may result in a disrupted velocity distribution across the duct section in which measurements are taken.



**Figure 2-7: Typical placement of holes for TAB procedures.**

To take advantage of pre-existing TAB conditions, a set of hot-wire velocity transducers, along with their velocity probes which are ideal for permanent installation per their manufacturer, was selected for the experiment. The devices have an accuracy of  $\pm 0.5\%$  of full scale of selected range and repeatability of less than  $\pm 1.0\%$  of reading. The response time is 0.2 seconds, which make them a great tool for monitoring the velocity variations in an airflow stream with great accuracy. The transducers also provide 4-20mA output signals.

### ***2.3.3 Holding bracket prototype***

In order to ensure a fixed position of the airflow measurement for extended measurement time, hot-wire probes adopted in this research work require the development of a portable holding bracket prototype (see Figure 2-8 (a)). With the implementation of this bracket, the airflow measurement probe can be held at a fixed depth in the ductwork for extended sampling times (see Figure 2-8 (b)). Additionally, human error factors are reduced

because the device will be holding the airflow measurement probe at fixed perpendicular angles to the airflow stream.

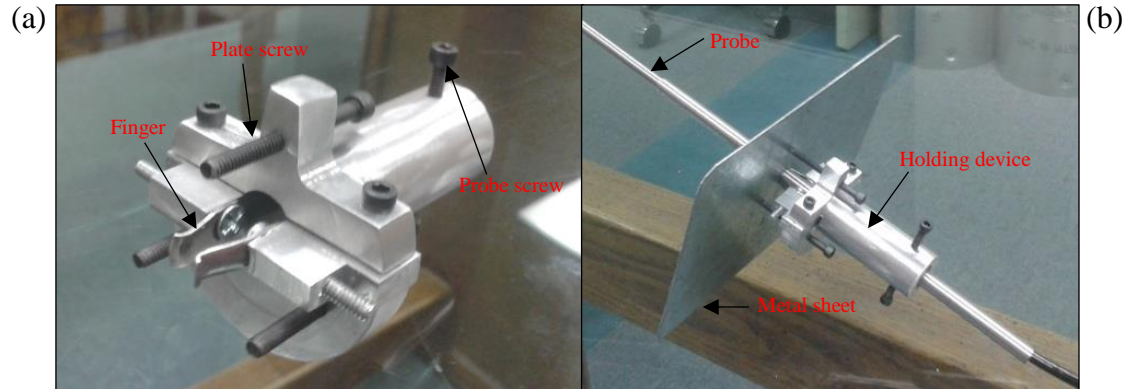


**Figure 2-8: Designed and manufactured holding bracket (Source: Rivas Prieto et al., 2016b).**

Figure 2-9 displays how the holding bracket helped to perform the in-situ airflow measurements in AHU-6.



**Figure 2-9: Hot-wire velocity probe mounting in AHU-6 for performing traverse measurements.**

### 2.3.4 Data acquisition devices

In order to log all the measurements for an extended period of time, separate data acquisition devices (DAQ) are needed. To achieve these goals, several 4-Channel Analog Data Loggers were used as the DAQ.

According to the manufacturer, the DAQ provides an accuracy of  $\pm 0.2\%$  of reading for a 4-20 mA input signal. The DAQ has the capability of instantaneous reading display and data storage at 1 second intervals for up to 5 days with 4 channels logging at the same time. The same loggers are also applied to log the fan head, fan speed and fan power measurements.

Figure 2-10 shows the adopted DAQ for recording airflow measurements from hot-wire velocity probes.



**Figure 2-10: Utilized DAQ for recording airflow measurements.**

## 2.4 Test Set-Up

Figure 2-11 shows the typical test set-up that is required for performing in-situ fan performance curve measurements in this thesis.



**Figure 2-11: Testing set-up for performing in-situ airflow measurements.**

The following steps describe the test set-up sequence required for generating in-situ fan performance curves.

1. *Placement of hot-wire velocity probes:* current industrial practice, traverse airflow measurements methods where a large number of sampling points are required, is intended for one operation measurement (usually at maximum design airflow rate) by TAB requirements. However, a one-point airflow rate calibration cannot provide full coverage of the wide operational scenarios of a fan. Therefore, a reduced number of sampling points need to be introduced to obtain continuous flow measurements for different fan operations. Chapter 3 will be focused on verifying uncertainties when a reduced number of sampling points is used to perform extended sampling time measurements under non-ideal measurement locations.

2. *Data recording devices set-up*: DAQs need to be set up for logging with 1 sec precision.
3. *Connect to BAS*: a laptop computer, containing a user interface to connect with the BAS and respective files for accessing each AHU control loop, needs to be connected to the AHU's control panel.
4. *VAV system override*: the VAV system's terminal units and boxes are fully opened for limiting airflow changes by fan speed changes only.
5. *BAS data recording*: temperature and pressure variables were monitored and recorded for accounting for any variation of conditions during the testing period.
6. *AHU override*: each fan of the VAV AHU will be overridden to defined speed combinations to obtain different ratios of the fan head over airflow squared. The procedure implemented in this thesis for defining these performance curves will be discussed in Chapter 4.

### **Chapter 3: Temporary Airflow Measurements for an Extended Time**

An airflow measurement with reduced sampling points for an extended time period needs to be defined and validated in this chapter. To understand the impacts of air velocity, traverse airflow measurement according to the Equal-Area method (see Figure 1-4) will be performed and recorded following initial experimental set-up, described in Section 2.4, as a reference. Then, in order to generate a wide range of airflow velocities in both SA and RA ductwork, different fan speeds (i.e., SF%/RF%: 95%/95%, 75%/75%, 50%/50% and 25%/30%) will be implemented. These fan speeds will generate a broad range of airflow velocities for each test AHU. This will allow the recording of necessary data for further analysis in order to validate the impacts of sampling time, reduced number of sampling points, and non-ideal measurement location on airflow measurements.

Therefore, the chapter is outlined as follows: first, Section 3.1 is focused on defining an ideal sampling time interval. The hypothesis is that with longer sampling time, fluctuations in the velocity profile can be captured. Second, in Section 3.2, uncertainties for different numbers of sampling points will be calculated and then compared to verify whether a minimum of 3 points can satisfy 5% accuracy criterion outlined by ASHRAE Standard 111 [2008]. This task will be achieved by implementing statistical analysis tools like root mean square errors (RMSE) and relative errors (RMSE%). Third, in Section 3.3, the impact of non-ideal measurement conditions on uncertainty for airflow measurements will be evaluated. Uncertainty results from test AHUs will be compared to check for the relationship of uncertainty as a function of different measurement locations. Last, in Section 3.4, a comparison of averages and accuracy of measurements between the 3-point



approach and typical airflow measurement device selected through industry guidelines is performed.

### **3.1.Sampling Time**

According to ASHRAE Standard 111 [2008] and the ASHRAE Fundamentals Handbook [2013a], with air flow fluctuations, the accuracy of air velocity measurements can be improved by time-averaging the readings or performing short succession consecutive traverse measurements. Generally, 2 or 3 seconds for a sampling time is suggested as a time-averaging interval for ensuring airflow measurement accuracy [TSI, 2012].

These general measurement guidelines explain how airflow measurements should be performed by technicians in the field, where they must manually hold the measurement device during the complete measurement procedure, point by point, in order to complete a traverse airflow measurement. This common method implies two main limitations and sources of errors for the airflow measurements:

1. Sampling time is limited by physical capabilities of the technicians who perform airflow velocity measurements by the traverse methods.
2. Accuracy of measurement devices is very sensible to the alignment between the airflow stream and device's measurement sensor. Thus, the technician's skills and experience are critical for ensuring accuracy of the airflow measurements.

These two limitations can be addressed by the implementation of the described holding bracket in Section 2.3. With this tool, the airflow measurement's sampling time can be extended and dependency on technicians is eliminated. Moreover, since the airflow

velocity will be recorded through DAQs, it is possible to analyze and compare the results from different sampling times (i.e., 2, 3, 4, 5, 10, 15, 20, 30, 45, 60 and 160 seconds).

Schwenk’s [1998] conclusions on airflow measurements show that comparable accuracy from 35 and 3 sampling points can be obtained for turbulent flows above 700 fpm. Increasing airflow velocity will increase turbulence of a flow stream and more uniform velocity distributions are generated. Therefore, 3 points at the highest possible airflow velocity are selected to investigate the accuracy of the reduced sampling point method by comparing them with the measurement results from full traverse sampling points.

As an example, Figure 3-1 shows the traverse sections for SA (see Figure 3-1 (a)) and RA (see Figure 3-1 (b)) of AHU-6 where, according to the traverse method, grids of 20 and 25 sampling points are required respectively.

In Figure 3-1 (b), D1 to D5 indicate the required depths and L1 to L5 indicate the required insertion lanes. Thus, each sampling point can be identified by a depth and lane (e.g., D2L2, D4L3, D3L4, etc.).

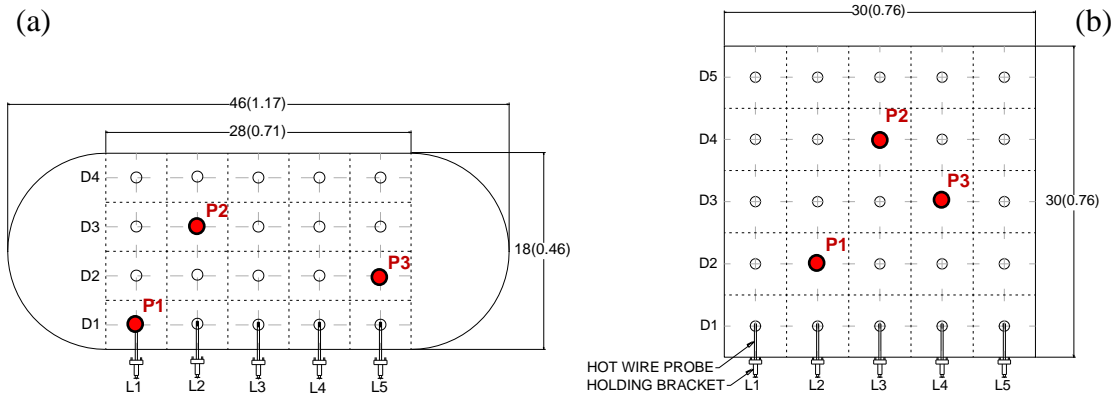


**Figure 3-1: Traverse grid for SA and RA sections in AHU-6 (Source: Rivas Prieto et al., 2016b).**

Then, airflow velocities from “n” (25 points in Figure 3-1 (b)) sampling points through traverse measurements can be obtained for each test AHU on the SA and RA sides. In addition, as displayed, 3 points (P1, P2 and P3) are also selected in the traverse grid. The selection is defined through the closest match between the average velocity by these 3 points and the average velocity using the traverse method at a 95% fan speed.

The measurement results and analysis of different sampling time impacts on the “n” sampling points and 3 sampling points for the three test AHUs described in Section 2.2 are compared in the sections below.

**3.1.1 AHU-5**

Figures 3-2 and 3-3 show the average velocity comparisons between the traverse and 3-point (3-P) method for SA and RA, respectively, at four different airflow velocities. Average velocities are presented with error bands based on 95% confidence.

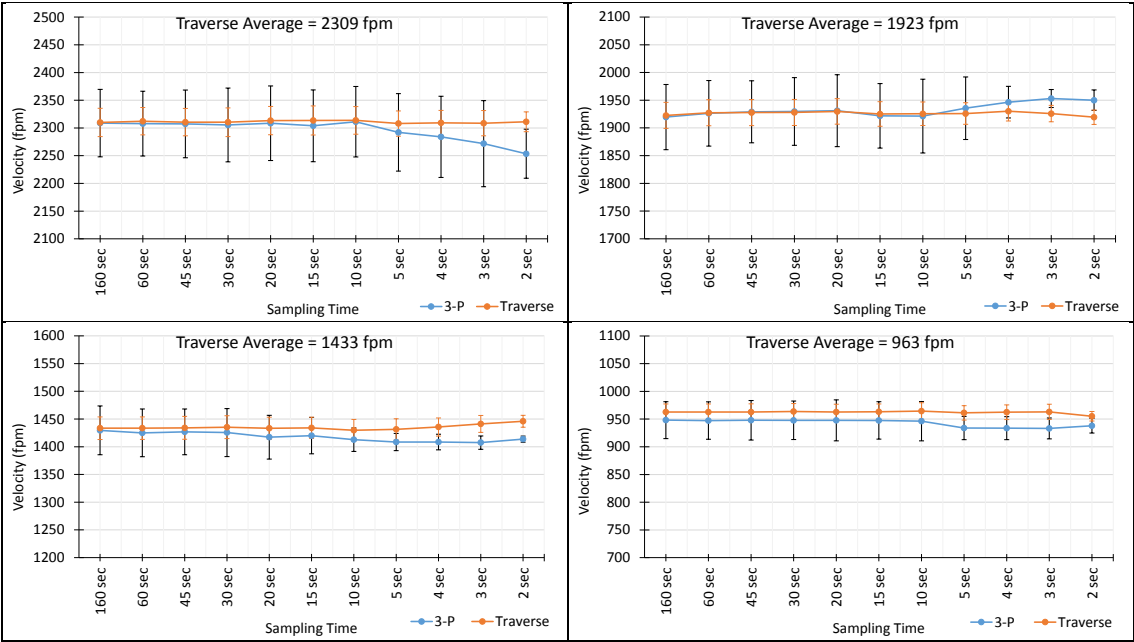


**Figure 3-2: Average velocity vs. sampling time by traverse and 3-P for SA AHU-5.**

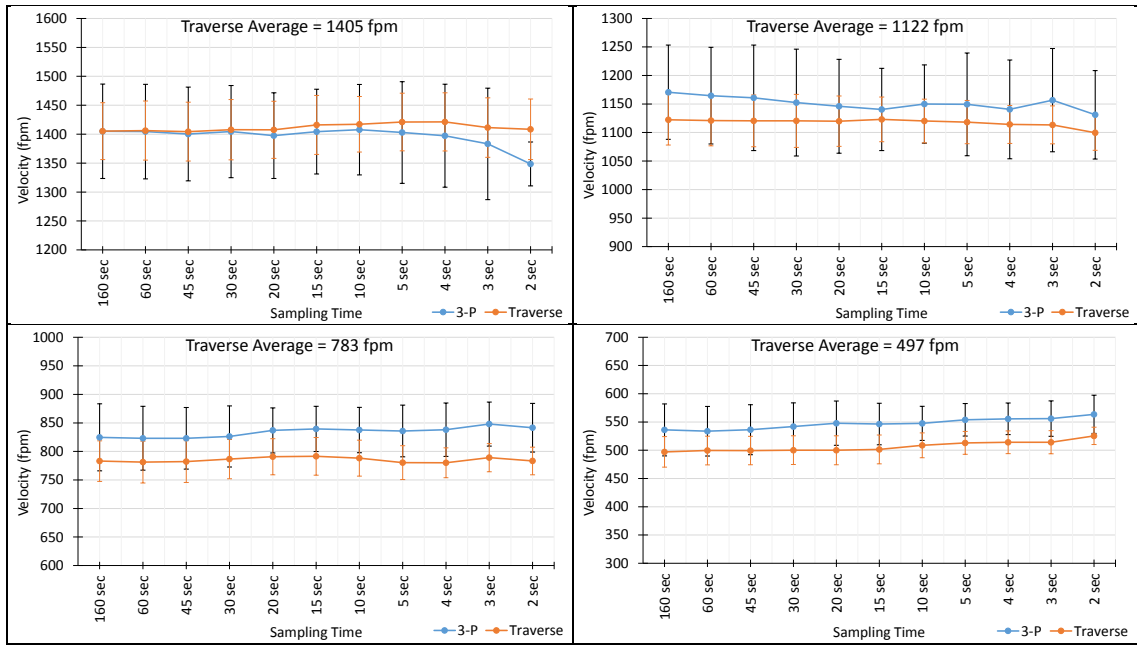


**Figure 3-3: Average velocity vs. sampling time by traverse and 3-P for RA AHU-5.**

While the longer sampling time results in little or no improvement to the average velocities that are obtained by the required traverse sampling points, significant improvement can be observed for the average velocity obtained by the three sampling points. For the 3-P measurements, when velocity is above 1405 fpm in SA or RA, the average airflow velocities are close to the values obtained by the traverse method when sampling time reaches 60 seconds. This is because the three points are selected by matching the average velocities between the traverse and the 3-P at highest velocity. On the other hand, when airflow velocity is lower than 1405 fpm, the 3-P method is not capable of reproducing the average airflow velocity by showing a constant bias between the two.

The constant bias between the averages suggests that the velocity distribution on the traverse plane experiences non-homothetic changes when airflow velocity is reduced, i.e., the selected three points are no longer representative of the average velocity in ducts when

the air velocity is significantly reduced. This occurs particularly because the disturbances in the flow stream create velocity vectors perpendicular to the inner wall of ductwork and a wake region. These velocity vectors and wake region produced by disturbances can create distortions in the velocity distribution, since the magnitude of the vectors and region changes with airflow velocity variations.

### 3.1.2 AHU-6

Figures 3-4 and 3-5 show the average velocity through the traverse measurement and the 3-P method for the SA and RA, respectively, for four different airflow velocities with several sampling times. Average velocities are presented with error bands based on 95% confidence.

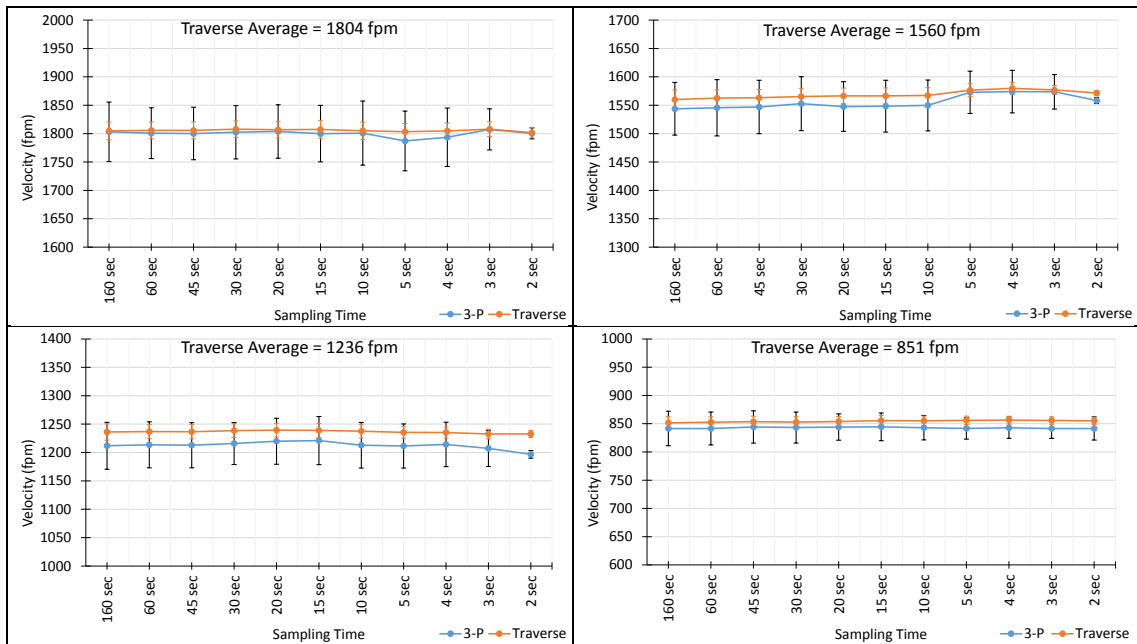
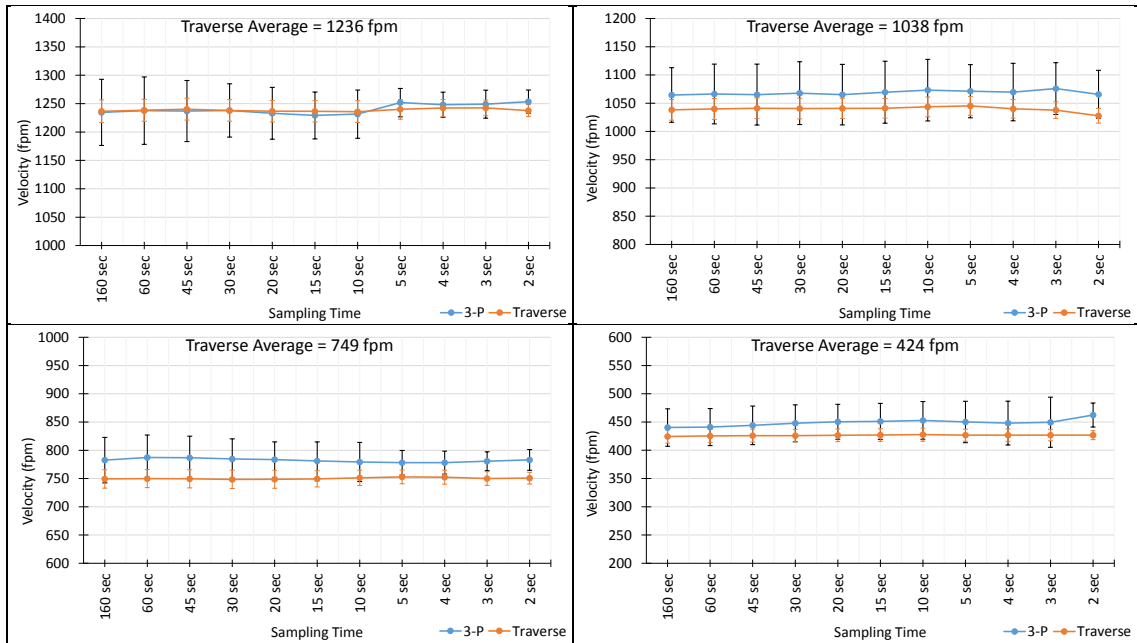


Figure 3-4: Average velocity vs. sampling time by traverse and 3-P for SA AHU-6.



**Figure 3-5: Average velocity vs. sampling time by traverse and 3-P for RA AHU-6.**

Similar to results in AHU-5, traverse average airflow velocity shows no significant improvement when sampling time is increased. Nonetheless, for 3-P measurements, improvement for sampling time above 30 seconds is observed at airflow velocities of 1804 and 1236 fpm for the SA and RA, respectively. This is explained by the selection of the three sampling points at highest velocity in such a way that their average matches the traverse method average. Conversely, when airflow velocity is reduced for SA and RA, the 3-P measurements are no longer effective in reproducing the average through the traverse method, since a constant bias develops between the 3-P and traverse methods due to a similar reason.

### 3.1.3 AHU-9

Figures 3-6 and 3-7 show the average velocity through traverse and 3-P methods for the SA and RA, respectively, for four different airflow velocities with different sampling times. Average velocities are presented with error bands based on 95% confidence.

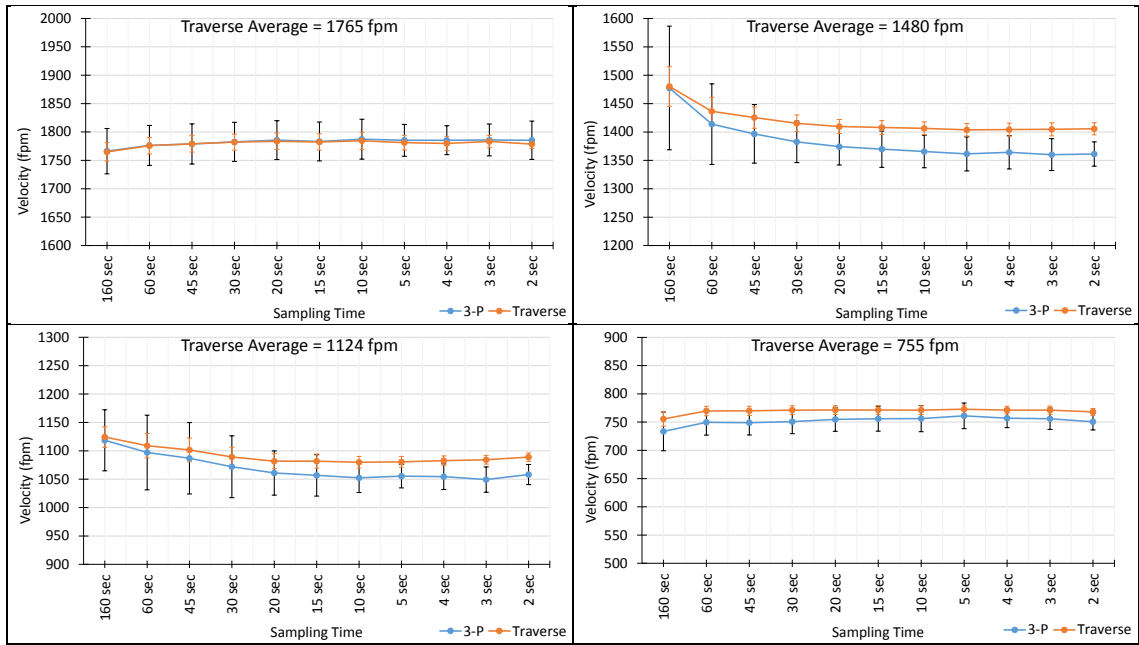


**Figure 3-6: Average velocity vs. sampling time by traverse and 3-P for SA AHU-9.**

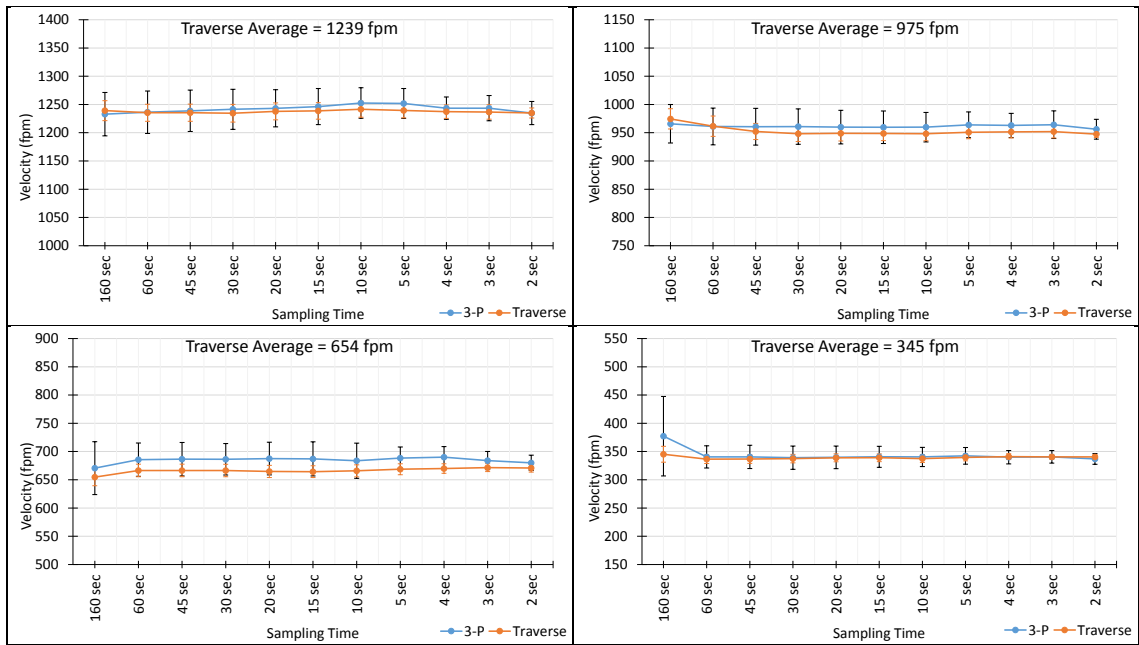


**Figure 3-7: Average velocity vs. sampling time by traverse and 3-P for RA AHU-9.**

Different from AHUs 5 and 6 where a longer sampling time does not have significant impacts on the traverse measurement results, for the SA and RA of this unit, AHU-9 shows that a longer sampling time causes significantly different results obtained by

different sampling times, even for the traverse method. To understand the different observations, the average velocity by traverse is plotted by a second interval in Figure 3-8.

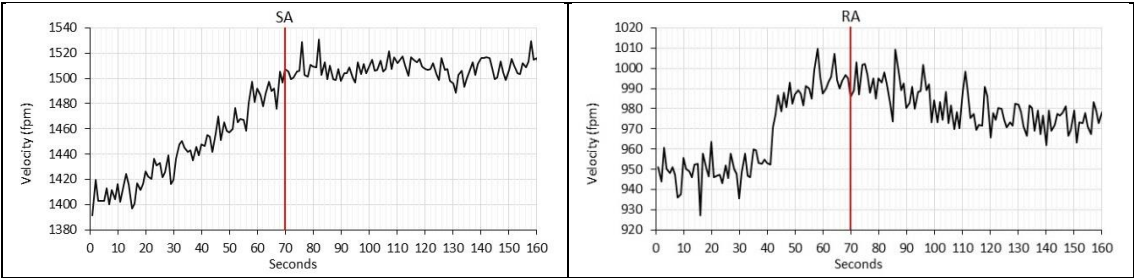


**Figure 3-8: Average velocity by traverse for SA at 1480 fpm and RA at 975 fpm during testing.**

While increasing sampling time helped improve the velocity’s fluctuation, it is observed that increasing sampling time above 60 seconds introduces variation effects of the VAV system in airflow measurements. This interesting finding suggests that although a longer sampling time eliminates the errors caused by flow turbulence for the reduced sampling point measurements, the sampling time cannot be so long that average velocities no longer represent true system dynamics, especially for a VAV system where flow rate changes constantly according to the variations of building loads.

Figure 3-8 shows that if measurements are analyzed from the 70<sup>th</sup> second for SA and RA, results similar to AHUs 5 and 6 would be obtained as the airflow velocity range stabilizes. Figure 3-9 shows the adjusted velocity graphs for different sampling times starting from the 70<sup>th</sup> second for the SA. A similar analysis is performed for RA-adjusted measurements.



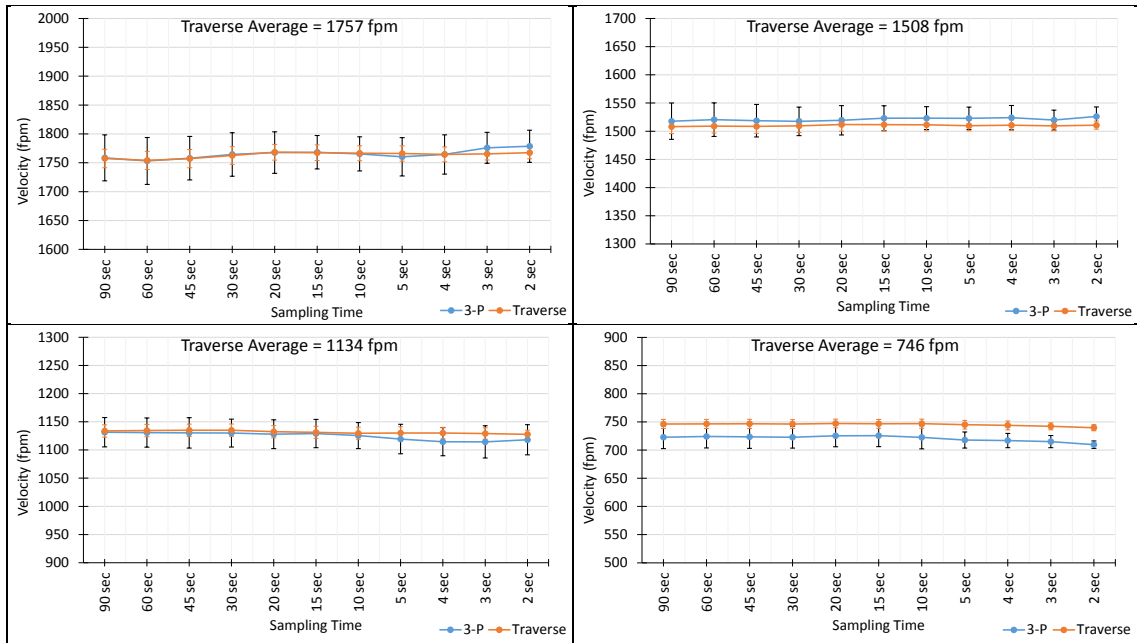


**Figure 3-9: Average velocity vs. sampling time from the 70th second by traverse and 3-P for SA AHU-9.**

Adjusted average velocity graphs for SA confirm that if variation effects are avoided, similar conclusions for the SA of AHUs 5 and 6 will be reached. In addition, a similar separation between 3-P and traverse methods averages is observed for a sampling time above 30 seconds at lower velocities. A constant bias is observed for extended sampling time when airflow velocities are 1508 and 746 fpm for the SA measurements. Similar conclusions will be reached for adjusted RA measurements.

### 3.1.4 Summary

To summarize obtained results from the test AHUs, Figure 3-10 shows the differences between average velocities (see Equation 3-1) obtained by the 3-P method at the different sampling times and the average obtained by the traverse at the longest sampling time for all tested cases categorized by SA and RA. Each line in Figure 3-10 is also labelled as the ratio of measured velocity over maximum airflow velocity tested in each case.

$$(3-1) \quad \text{Relative Difference (\%)} = \frac{\frac{\sum_1^n v_{i@160ref.time}}{n} - \frac{\sum_1^3 v_{i@sampling.time}}{3}}{\frac{\sum_1^n v_{i@ref.time}}{n}} \times 100\%$$

where  $v_{i@ref.time}$  = airflow velocity per sampling point at the reference sampling time,  
 $v_{i@sampling.time}$  = airflow velocity per sampling point at different tested sampling times,  
and  $n$  = the number of sampling points by the traverse method.

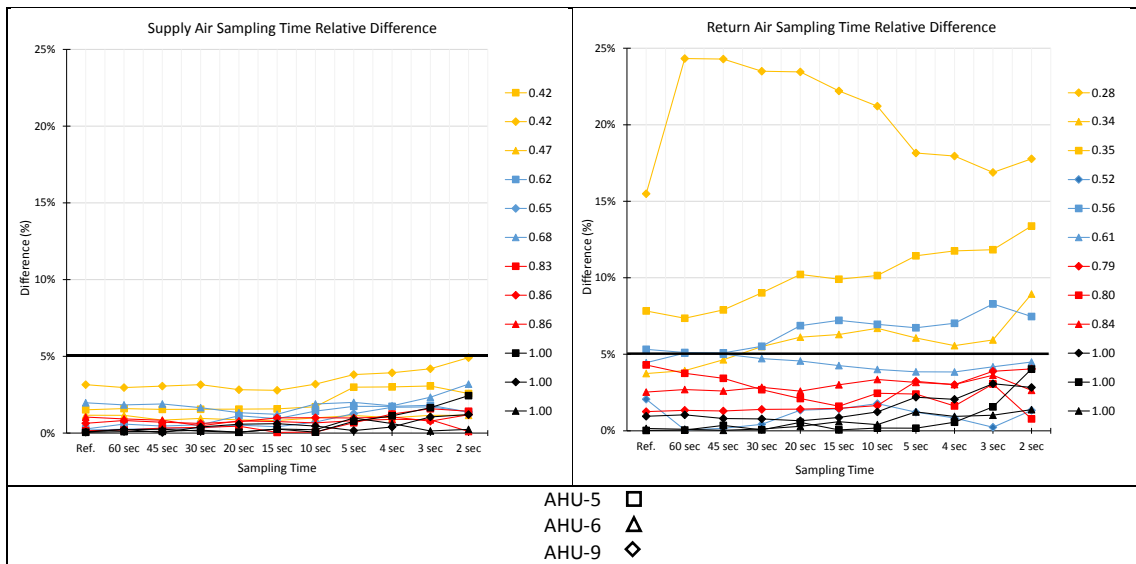


**Figure 3-10: Comparisons of 3-P vs. traverse relative differences for SA and RA measurements.**

Based on the results in Figure 3-10, it is possible to make the following observations:

- In general, the error impact of oscillations on velocity measurements can be significantly reduced by increasing sampling time up to 60 seconds for the 3-P measurements, while a 2-3 second sampling time is still viable for the full traverse measurements. Increasing sampling time up to 60 seconds allows reducing relative differences in 3-P average velocities equal or below 5% (required accuracy by ASHRAE Standard 111 [2008]) for all the SA measurements and the majority of the RA measurements.

- The reduced errors are velocity-dependent. Constant biases exist as the velocity reduces when comparing 3-P measurements with the traverse measurements. It is concluded that the three points cannot consistently represent the average velocity when the flow velocity changes. This is because the non-homothetic velocity distribution changes when flow rate reduces.
- The error reduction of the longer sampling time method is more effective on the SA than on the RA measurements. The larger errors on the RA are from the constant bias. In other words, there is less chance to maintain homothetic velocity distribution changes in the RA than in the SA due to much lower velocities in the RA.
- Sampling time above 60 seconds in VAV systems can lead to additional uncertainty in airflow velocity averaging due to inclusion of system variation effects.
- Extraordinary large errors (up to 20%) can be observed for the RA when the velocities are lower than 400 fpm. By the observation, the data that show higher than 5% errors in Figure 3-10 are all with less than 800 fpm velocity.

In conclusion, a 60-second sampling time is suggested as an appropriate time interval to eliminate the flow oscillation impacts on the measurements that cannot be captured due to the reduced number of the sampling points.

### **3.2 Sampling Points**

A reduced number of sampling points is suggested in order to obtain average airflow velocity for an extended period of time. As discussed in Section 3.1, when 3-P method

was used, because the three selected points cannot always represent the average velocity in ducts when velocities change, some uncertainty was introduced to the measurements due to additional uncertainties introduced by fewer sampling points.

Under ideal or non-ideal measurement conditions, each measurement sampling point can have non-homothetic behavior depending on disturbances and the system design. Therefore, when a reduced number of sampling points is applied, the obtained average airflow velocity is sensible to the point selection. Thus, additional uncertainty introduced by non-homothetic velocity profiles needs to be defined and considered.

In this section, we will extend our study to 5-point (5-P) and 9-point (9-P) methods in addition to the 3-P method. Following the same principle for the 3-P selection in Section 3.1, five representative points and nine representative points are selected for 5-P and 9-P methods by matching the averages between the average of the selected points and that of the traverse.

To verify and validate the reduced number of sampling points, some analysis tools need to be defined first:

Bias introduced by reduced sampling points: consistent biases were observed for 3-P measurements at 4 different airflow velocities in both SA and RA for each AHU in Section 3.1. Root mean square error (RMSE) allows comparing the reduced-point measurements to the traverse measurements at each test velocity and summarizing for an overall bias for SA and RA, respectively. With this approach, results from different AHUs can be fairly compared. Equation 3-2 shows the RMSE formulation for this study.

$$(3-2) \quad RMSE = \sqrt{\left(\sum_{i=1}^{i=n} (\bar{v}_{i(m)} - \bar{v}_{i(traverse)})^2\right)/n}$$

where  $n$  = total of tested fan speeds,  $m$  = number of sampling points,  $\bar{v}_{i(m)}$  = average airflow velocity for reduced sampling points at a constant fan speed, and  $\bar{v}_{i(traverse)}$  = average airflow velocity by traverse method for a constant fan speed.

A relative error introduced by reduced sampling points: uncertainty of non-homothecy analysis on velocity distributions is required for each test AHU due to a reduced number of sampling points. Ideally, the ratio of reduced sampling point measurement over the traverse measurements should be 1 if the velocity changes are homothetic by the flow rate variations, i.e., the greater the distance of the ratio from 1, the larger the non-homothetic changes. Therefore, Equations 3-3 and 3-4 are defined to show the uncertainty of non-homothetic velocity distributions.

$$(3-3) \quad \widehat{v}_n = \frac{\bar{v}_{n(m)}}{\bar{v}_{n(traverse)}}$$

where  $\widehat{v}_n$  = normalized airflow velocity for a constant fan speed.

$$(3-4) \quad RMSE\% = \sqrt{\left(\sum_{i=1}^{i=n} (\widehat{v}_i - 1)^2\right)/n} \times 100\%$$

where  $RMSE\%$  = relative error due to non-homothetic velocity distribution expressed as percentage.

As an example, if analysis tools are applied on the Figure 3-1 section, variables would be named as follows for 25% constant fan speed and 5-Point analysis:

- $\bar{v}_{i(traverse)} = \bar{v}_{1(traverse)}$  refers to average airflow velocity through traverse for 25% fan speed (i=1).
- $\bar{v}_{i(m-p)} = \bar{v}_{1(5-p)}$  refers to the average airflow velocity through 5-Point that we will need to compare to it.
- $\widehat{v}_n = \widehat{v}_1$  indicates the normalized value for 25% of fan speed.

### 3.2.1 AHU-5

Tables 3-1 and 3-2 show the calculated 3-P and traverse airflow velocities in Section 3.1 for AHU-5. In addition, results from applying the 5-P and 9-P methods are displayed.

**Table 3-1: Reduced number of sampling points analysis for SA AHU-5.**

Fan Speed	Traverse (fpm)	60 seconds		
		3-P (fpm)	5-P (fpm)	9-P (fpm)
95%	2309.43	2305.20	2310.63	2313.99
75%	1922.43	1924.57	1924.05	1935.81
50%	1432.78	1449.54	1420.10	1434.48
25%	963.16	978.48	947.16	961.27
RMSE (fpm)		11.60	10.26	7.18
RMSE%		0.99%	0.94%	0.38%

**Table 3-2: Reduced number of sampling points analysis for RA AHU-5.**

Fan Speed	Traverse (fpm)	60 seconds		
		3-P (fpm)	5-P (fpm)	9-P (fpm)
95%	1405.03	1398.57	1400.86	1400.78
75%	1120.39	1162.95	1141.66	1117.62
50%	785.92	822.77	802.35	785.33
25%	496.49	533.77	513.35	510.20
RMSE (fpm)		33.91	16.00	7.32
RMSE%		4.82%	2.21%	1.40%

Based on obtained results from analyzing calculated average velocities through 3, 5 and 9-Point methods, the following facts can be outlined:

- RMSE% values below 5% criterion are observed for SA and RA when airflow measurements are performed through 3, 5 and 9-Point methods, although the RA shows more non-homothetic behaviors by much larger RSME% than the ones on the SA.
- Results for AHU-5 show that when the reduced sampling point method is applied, increasing the number of sampling points can reduce error and uncertainty.

### 3.2.2 AHU-6

Tables 3-3 and 3-4 show the calculated 3-P and traverse airflow velocities in Section 3.1 for AHU-6. In addition, results from applying the 5-P and 9-P methods are displayed.

**Table 3-3: Reduced number of sampling points analysis for SA AHU-6.**

Fan Speed	Traverse (fpm)	60 seconds		
		3-P (fpm)	5-P (fpm)	9-P (fpm)
95%	1803.53	1800.82	1813.06	1802.63
75%	1558.73	1545.60	1578.19	1555.19
50%	1236.27	1213.53	1255.47	1232.62
25%	851.32	841.50	872.15	852.20
RMSE (fpm)		14.08	17.83	2.62
RMSE%		1.17%	1.60%	0.19%

**Table 3-4: Reduced number of sampling points analysis for RA AHU-6.**

Fan Speed	Traverse (fpm)	60 seconds		
		3-P (fpm)	5-P (fpm)	9-P (fpm)
95%	1236.61	1237.72	1236.66	1238.53
75%	1038.14	1066.31	1055.75	1032.08
50%	749.16	787.26	755.58	747.07
25%	424.34	441.09	443.45	411.19
RMSE (fpm)		25.13	13.38	7.38
RMSE%		3.49%	2.44%	1.59%

Based on the obtained results from analyzing calculated average velocities through 3, 5 and 9-Point methods, the following facts can be outlined:

- While a significant improvement in accuracy is obtained for SA measurements when the 9-P method is applied instead of the 3-P method, a slight decrease in accuracy is observed when the 5-P method is applied. This suggests that selecting a greater number does not guarantee improvements in accuracy. This is because selecting greater number of sampling point can suggest considering additional points with highly non-homothetic behavior that introduces more uncertainty to the calculated average velocity.
- RMSE% showed compliance with ASHRAE Standard [2008] 5% required accuracy regardless of the tested number of sampling points.

### 3.2.3 AHU-9

Tables 3-5 and 3-6 show the calculated 3-P and traverse airflow velocities in Section 3.1 for AHU-9. In addition, the results from applying the 5-P and 9-P methods are displayed.

**Table 3-5: Reduced number of sampling points analysis for SA AHU-9.**

Fan Speed	Traverse (fpm)	60 seconds		
		3-P (fpm)	5-P (fpm)	9-P (fpm)
95%	1756.99	1745.11	1741.79	1737.98
75%	1506.56	1518.90	1497.84	1499.10
50%	1134.18	1134.97	1124.09	1133.53
25%	746.63	747.43	723.62	756.96
	RMSE (fpm)	8.58	15.32	15.50
	RMSE%	0.53%	1.69%	0.98%

**Table 3-6: Reduced number of sampling points analysis for RA AHU-9.**

Fan Speed	Traverse (fpm)	60 seconds		
		3-P (fpm)	5-P (fpm)	9-P (fpm)
95%	1238.51	1233.51	1233.51	1239.26
75%	981.07	969.08	986.65	996.90
50%	648.98	674.97	652.37	654.78
25%	351.63	372.33	340.01	352.27
	RMSE (fpm)	17.84	7.12	8.45
	RMSE%	3.62%	1.71%	0.93%



Similar conclusions to AHUs 5 and 6 can be reached regarding SA and RA measurements. It is noted that the obtained RMSE% for SA measurements is the lowest among all cases. These facts suggest that homothetic profiles are being tested in SA. However, it is observed that increasing the number of sampling points generates a slight increase of RMSE%.

Measurements on RA show lower RMSE% values when increasing sampling points. This suggests that isolated sampling points are not being accounted for in the average velocity. It also suggests that at lower velocities in turbulent flows, isolation of sampling points is less probable than at higher velocity ranges.

### 3.2.4 Summary

Table 3-7 shows the results for the test AHUs.

**Table 3-7: Summary of RMSE and RMSE%.**

Side	AHU	RMSE (fpm)			RMSE%		
		3-P	5-P	9-P	3-P	5-P	9-P
RA	5	33.91	16.00	7.32	<b>4.82%</b>	2.21%	1.40%
	6	25.13	13.38	7.38	<b>3.49%</b>	2.44%	1.59%
	9	17.84	7.12	8.45	<b>3.62%</b>	1.71%	0.93%
SA	5	11.60	10.26	7.18	<b>0.99%</b>	0.94%	0.38%
	6	14.08	17.83	2.62	<b>1.17%</b>	1.60%	0.19%
	9	8.58	15.32	15.50	<b>0.53%</b>	1.69%	0.98%

Analysis of 3-P, 5-P and 9-P measurements shows that uncertainties are not exceeding 5% ASHRAE Standard 111 [2008] criterion in any case. In some cases, results for the 5-P and 9-P methods show slightly larger uncertainties than the 3-P measurements for the SA measurements. This indicates that when the velocity is high, at 800 fpm or above, increasing the sampling points from 3 to 5 does not significantly improve the measurement. However, for the RA measurements, where the velocity is generally lower

(less than 800 fpm in the most case), the 5-P method can reduce the RSME% by nearly half, and 9-P can reduce RSME% by another one-half.

### 3.3 Location Factor

Previous research has suggested that a relationship between the measurement location and uncertainty in airflow measurement may exist. Rivas Prieto et al. [2016a] suggest that based on ASHRAE-required straight duct lengths as a reference (see Table 2-2), compromised straight duct lengths can be defined as a location factor (see Equation 3-5), which is calculated using the summed ratios of compromised duct lengths from both the downstream and upstream fittings from the TS. Obtained location factors for both SA and RA of each AHU are listed in Table 3-8.

$$(3-5) \quad \text{Location factor} = \sum_j^2 \max(0, (L_{req,j} - L_{actual,j}) / L_{req,j})$$

where j=downstream or upstream;  $L_{req}$ =required length by ASHRAE; and  $L_{actual}$ =actual length.

**Table 3-8: Percentages of compensated straight duct lengths (Source: Rivas Prieto et al., 2016a).**

AHU	SA			RA		
	A	B	Location factor	E	F	Location factor
5	0.817	0.900	1.717	0.822	0.831	1.653
6	0.085	0.520	0.605	0.889	0.782	1.671
9	0.100	0.160	0.259	0.968	0.927	1.894

For SA measurements, it is possible to observe a wide range of values for the location factor. AHU-9 is the best case, with a location factor of 0.259, and AHU-5 is the worst, with a location factor of 1.717. Since such a large difference exists for the SA measurement locations, the study for verifying the impact of measurement location will be focused just on SA.

In order to investigate the impact of close disturbances on sampling points experiencing non-homothetic effects, the velocity measured by each probe at time  $\tau$  was normalized using the velocity at the same time  $\tau$  of the probe that contains the majority of the maximum velocities among the three probes in the same ducts, by Equation 3-6.

$$(3-6) \quad \bar{v}_{t,k} = \frac{v_{t,k}}{\max(v_{t,A})}$$

where  $t$ =measurement sample at time  $\tau$  for each probe;  $k=1$  to 3 for three sampling probes; and  $A$ =the probe that contains most of the maximum velocity measurements among the three probes.

The normalized velocities of AHU-6 for airflow measurements taken during continuous operation are shown in Figure 3-11. If the velocity distribution on a traverse plane changes homothetically, then all three lines should be horizontal or constant. As Figure 3-11 illustrates, this is not true, especially when the velocity goes below 1500 and 1000 fpm in SA and RA, respectively.

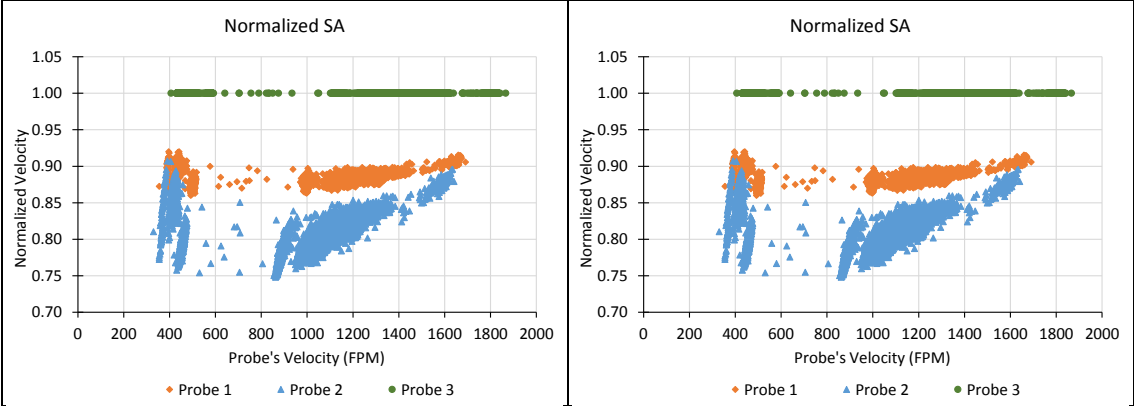


**Figure 3-11: Normalized velocity for SA and RA in AHU-6.**

Since the velocity distribution changes are non-homothetic under different airflow rates, the normalized velocity for each probe shows deviations from a constant over time when

air velocity changes. The root mean square error ( $RMSE_k$ ) of normalized velocities for each probe is used to measure the differences between the sample values at each time  $\tau$  with the population means. The  $RMSE_k$  of normalized velocities for each probe is calculated using Equation 3-7.

$$(3-7) \quad RMSE_k = \sqrt{\sum_{t=1}^{M_k} (\bar{v}_{t,k} - \bar{v}_{avg,k})^2 / (M_k - 1)}$$

where  $M_k$ =population size for each probe measurement.

The larger the  $RMSE_k$  is, the more non-homothetic the velocity distribution change is. Then, since there are three  $RMSE_k$  values obtained by three different probes in each test AHU, root mean square averages are applied to find the combined  $RMSE_k$  (see Equation 3-8) for each SA and RA measurement of each AHU.

$$(3-8) \quad Combined\ RMSE_k = \left[ \frac{1}{n} \cdot \sqrt{\sum_{i=1}^{i=n} RMSE_{k,i}^2} \right] \times 100\%$$

where  $n$ = number of velocity probes and  $RMSE_{k,i} = RMSE_k$  for each velocity probe.

Results of calculating the combined  $RMSE_k$  for 3-P measurements are summarized and organized by location factor in Figure 3-12.

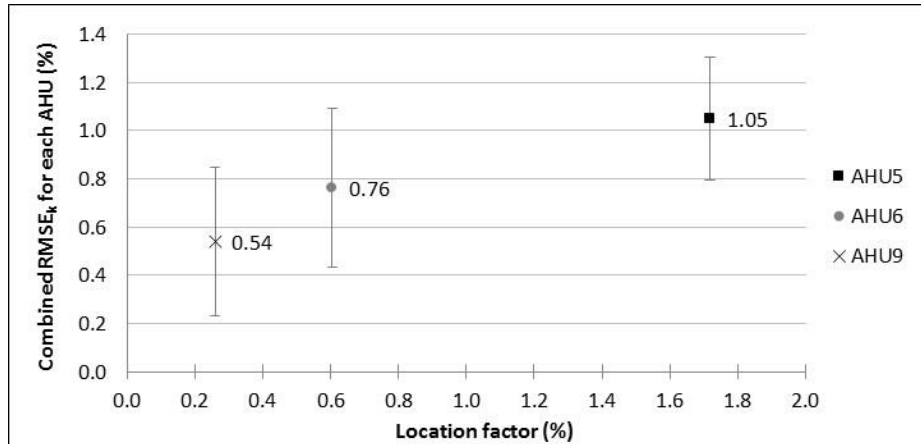


**Figure 3-12: Combined RMSE<sub>k</sub> vs. location factor (source: Rivas Prieto et al., 2016a).**

It is clear that the combined RMSE<sub>k</sub> increases as the location factor increases. The highest value of 1.05% is for AHU-5, where the location factor reaches 1.717. AHU-9 has the least combined RMSE<sub>k</sub> value of 0.54%, as the location factor is the smallest.

Results in Figure 3-12 show that a small location factor, i.e., closer to ideal upstream and downstream distances to disturbances, can improve the accuracy of airflow measurements. On the other hand, when the disturbance is closer to the traverse plane of measurement, i.e., a larger location factor, higher uncertainties due to non-homothetic velocity distributions are expected.

### **3.4 Industry Standard Thermal Sensor Measurements**

Permanent airflow measurements are needed in field applications for calibration and control of HVAC systems according to the ASHRAE HVAC Systems and Equipment Handbook [2016]. Different designs and performances can be obtained depending on the manufacturer; nevertheless, similar types will provide close uncertainties.

Appendix B shows that manufacturers ensure accuracy of 3% for common thermal dispersion airflow measurement stations (AFMS), while distances to disturbances are as short as 0.5 hydraulic diameters. In addition, an industry guideline for choosing the number and location of sampling points is suggested.

Then, based on guidelines from Appendix B, sampling points can be selected (see Figure 3-13 (a) and (b)) from the traverse measurement data sets obtained for Section 3.1. Consequently, it will be possible to show an average velocity calculated through common industry applied AFMS). 3-P measurements from Section 3.2 can then be compared to the obtained average velocities through AFMS for each test AHU case. Accuracies for in-situ measurements through AFMS guidelines can then be evaluated and compared to obtained results by the 3-P method.

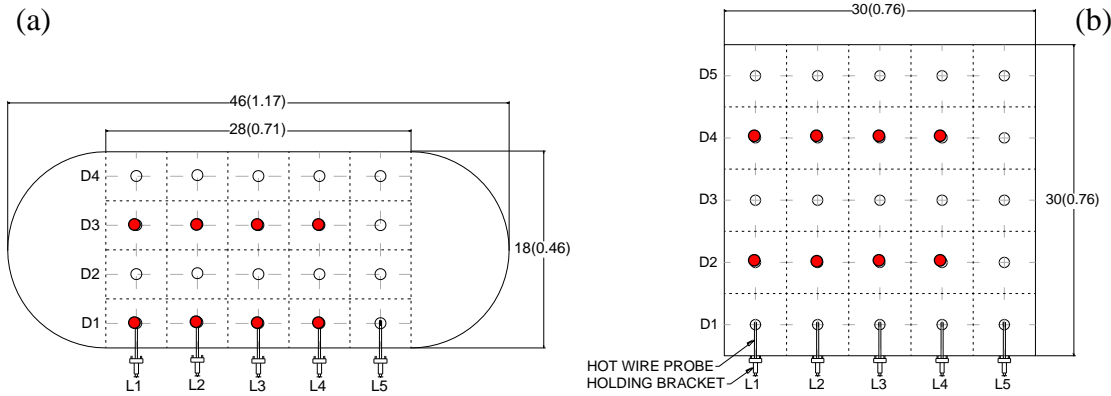


**Figure 3-13: AFMS sampling point locations for SA and RA of AHU-6.**

### 3.4.1 AHU-5

Figure 3-14 shows 3-P and AFMS airflow velocities vs. traverse measurements. The number of sampling points for the AFMS depends on the cross-sectional area (see Appendix B). For cross-sectional areas of 4.68 and 6.25 ft<sup>2</sup> for SA and RA, respectively, 8 sensor nodes will be required in each case.

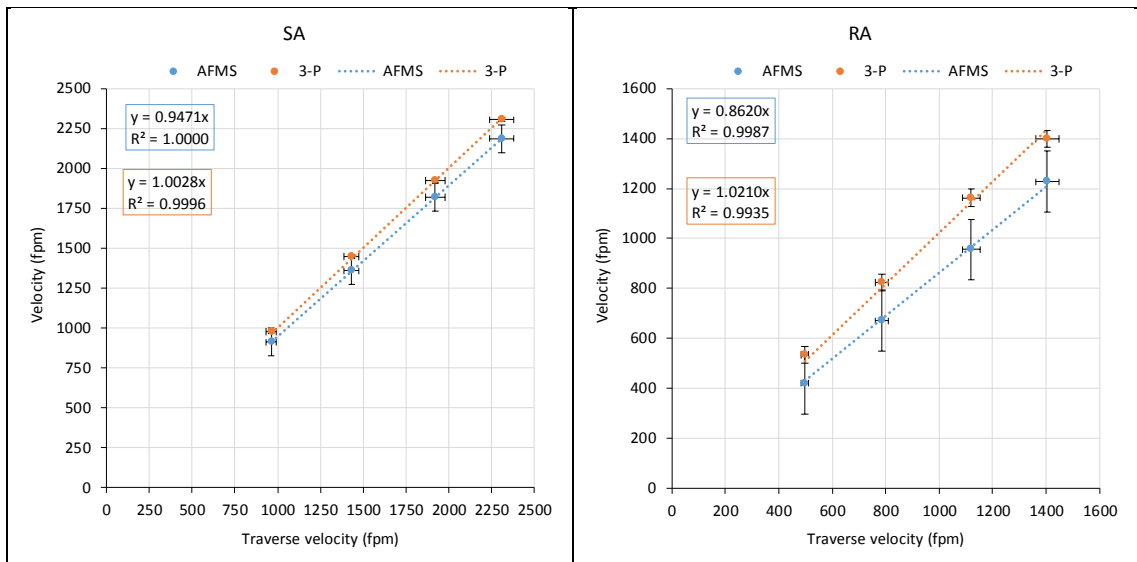


Figure 3-14: SA and RA by 3-P and AFMS comparison to traverse for AHU-5.

While SA measurements show that close results can be obtained through 3-P and AFMS methods, RA measurements show that AFMS is not able to provide results close to measurements by the 3-P method. Ideally, the slope of the linear fitting of airflow velocity should be 1. Nonetheless, AFMS differs from this value by 13.8% while the 3-P measurements slope is 2.1% off.

Additionally, it is possible to observe that uncertainty bands on RA measurements are larger than SA. Uncertainty bands are much smaller for 3-P measurements than they are for AFMS measurements. This suggests that a traverse calibration is always needed if sampling points are less than required by the traverse.

### 3.4.2 AHU-6

Figure 3-15 shows 3-P and AFMS airflow velocities compared to traverse measurements. The number of sampling points for the AFMS depends on the cross-sectional area (see Appendix B). For cross-sectional areas of 5.27 and 6.25 ft<sup>2</sup> for SA and RA, respectively, 8 sensor nodes will be required in each case.

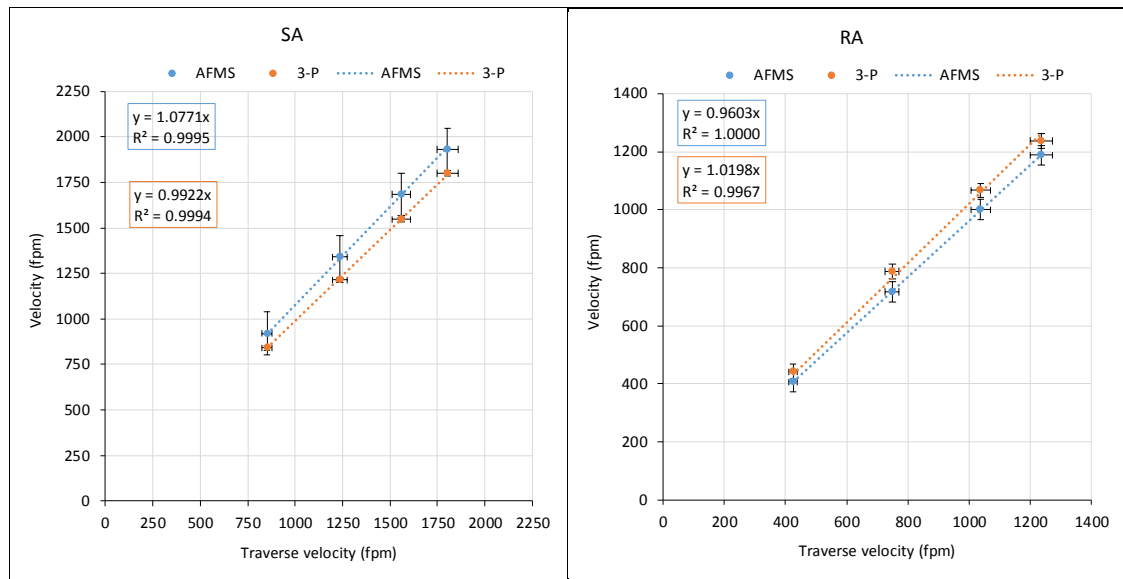


**Figure 3-15: SA and RA by 3-P and AFMS comparison to traverse for AHU-6.**

Similar conclusions to AHU-5 can be reached for SA measurements. Nonetheless, RA measurements show that 3-P and AFMS methods offer closer results than SA. Additionally, uncertainty bands are smaller on RA measurements when they are compared to SA.

Nevertheless, when AFMS measurements are compared to 3-P average velocities, it is possible to observe that in both SA and RA measurements, the 3-P methods generate slopes closer to 1 than AFMS measurements do. For example, for SA measurements, while the AFMS slope is 7.0% off, the 3-P measurements trend line is only 0.8% off.



### 3.4.3 AHU-9

Figure 3-16 shows the 3-P and AFMS airflow velocities compared to traverse measurements. The number of sampling points for the AFMS depends on the cross-sectional area (see Appendix B). For cross-sectional areas of 4.51 and 6.86 ft<sup>2</sup> for SA and RA, respectively, 8 sensor nodes will be required in each case.

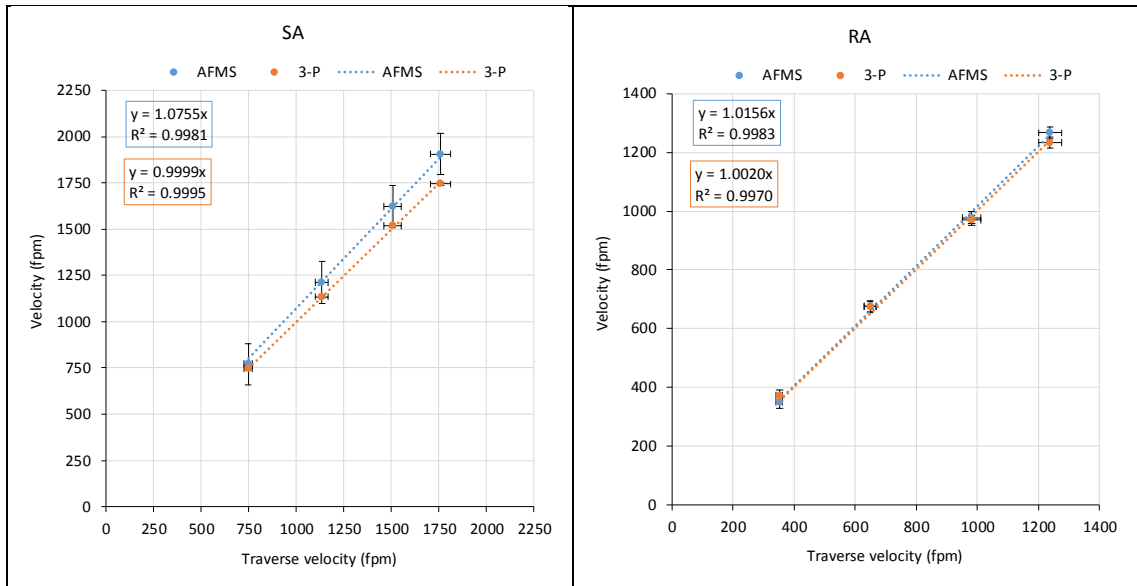


**Figure 3-16: SA and RA by 3-P and AFMS comparison to traverse for AHU-9.**

Similar conclusions to AHUs 5 and 6 can be reached for SA measurements. The AFMS method offers larger uncertainty bands than 3-P measurements do. Additionally, while the fitting for 3-P measurements is matching the traverse average velocities, the AFMS measurements trend line is 7.6% off from traverse measurements. For RA measurements, similar to AHU-6, 3-P and AFMS measurements offer close average velocities. Nevertheless, the uncertainty band is still larger in AFMS measurements than for the 3-P method. Finally, while the slope for average velocities through the 3-P method almost matches the traverse measurements with a 0.2% difference in slope, AFMS generates a slope that is 1.6% off from ideal values.

### 3.4.4 Summary

Common industry procedures for in-situ TAB suggest installing permanent AFMS devices for control and operation purposes. While these common devices can reduce installation costs by reducing the number of sampling points, obtaining in-situ airflow measurement accuracies below 5% ASHRAE Standard 111 [2008] criterion represents a major challenge. In multiple studies, the obtained slope for AFMS measurements was found to be equal or larger than 5% off from expected measurements through the traverse method if a traverse calibration was not performed first. Figure 3-17 shows the residuals from the comparison of obtained slopes for both AFMS and 3-P methods to an ideal matching traverse measurements, i.e., slope equal to 1.

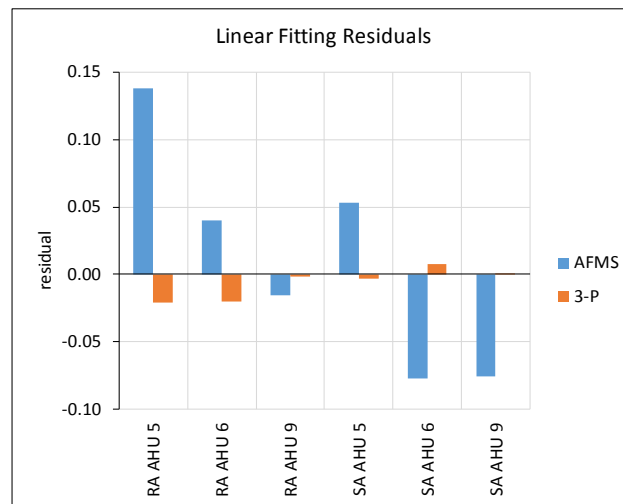


**Figure 3-17: Linear fitting residuals for 3-P and AFMS compared to traverse measurements.**

Since the residual is calculated based on a magnitude of 1, it can be also seen as a percentage. Therefore, considering the 5% accuracy criterion, i.e., residual of 0.05, it is possible to observe that AFMS measurements do not fall within the accuracy criterion for SA measurements. Additionally, divergent results are obtained for RA measurements. While RA measurements on AHUs 6 and 9 fall within the 5% range, measurements for

AHU-5 are 13.8% off from the ideal matching to traverse. On the other hand, 3-P measurements for RA or SA provide consistent matching to expected airflow velocities by the traverse method. These results suggest that a full-traverse calibration is always needed for any AFMS if the sampling points are less than required by traverse.

## Chapter 4: In-situ Fan Curve Calibration of VAV AHU

Fans are tested by manufacturers following common industry standards such as ANSI/ASHRAE Standard 51 to provide design engineers with reliable data for selecting an adequate fan for each HVAC system. The testing procedures are designed to generate a set of fan performance curves as presented in Figure 2-1. In general, ANSI/ASHRAE Standard 51 [1999] presents the minimum straight and non-obstructed duct lengths that are required at the traverse plane of measurement for testing fans in laboratory conditions (see Figure 4-1).

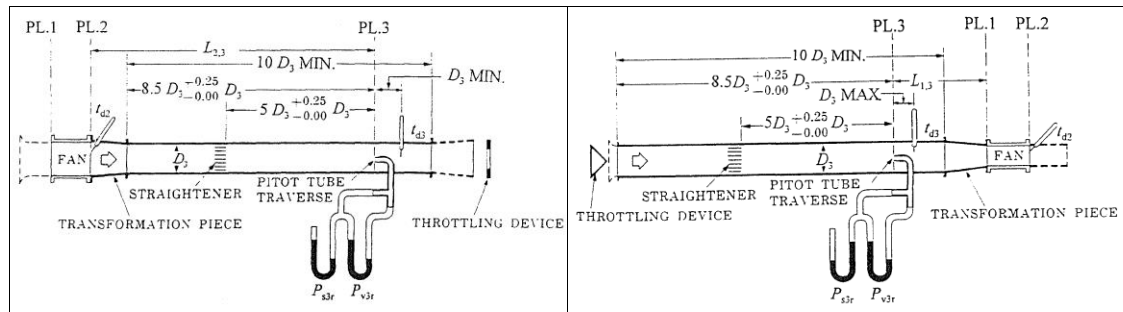


**Figure 4-1: Laboratory testing requirements for the outlet and inlet of fans (Source: ASHRAE, 1999).**

While described conditions can be perfectly applied in laboratory testing, they are not usually achievable in the field. In addition, disturbances in the airflow stream create distorted velocity distributions and pressure losses with significant impacts on fan performance, i.e., system effects [ASHRAE, 2016], different from the lab fan operations. Because field conditions strongly affect equipment performance, ASHRAE's HVAC Systems and Equipment Handbook [2016] suggests performing in-situ testing to obtain fan performance curves.

Section 4.1 will first introduce a customized calibration procedure for VAV AHUs. Then, Section 4.2 will detail the uncertainty analysis calculation procedure. Finally, Section 4.3 will present fan performance curves for test AHUs based on the 3-P method for airflow measurements.

#### **4.1 Calibration Procedure**

A customized procedure for calibrating in-situ VAV AHUs is needed in order to obtain in-situ fan performance curves with good accuracy. Research performed by Rivas Prieto et al. [2016b] included the calibration of VAV AHUs for obtaining these curves when the 3-P method is applied for airflow measurements.

For each test AHU shown in Table 2-1, since both the supply and return air fans are installed, different ratios of the fan head to the square of airflow for the supply and return air ducts can be obtained by overriding the supply and return air fan speed with different combinations. Accordingly, the summarized fan operation overrides can be found as follows:

1. Close the OA damper to make the SF and RF work in series in a single loop under identical airflow rates.
2. Set the RF at 100% of speed and modulate the SF speed by 10% for each step change until the measured differential pressure for the RF is close to zero. The high SF speed has to be regulated against the static pressure in the supply duct, since high static pressure could trip the AHU by the high static pressure switch. These overrides generate the full operational ranges for the RF and partial operational points for the SF.

3. When the SF speed reaches the highest point, reduce the RF speed at every 10% speed step to capture the full operational points for the supply air fan.
4. Maintain each speed combination for 10 minutes to collect sufficient data. This recording time will make the data robust enough to lower the random error in the airflow measurement.
5. Release the system from the override at the low fan speeds to ensure safe unit operations after the override is released.

## **4.2 Uncertainty Analysis**

Propagation of uncertainty analysis is required to obtain uncertainty bands for fan head vs. airflow and for fan efficiency vs. airflow curves. In the first place, airflow, fan head, and fan power are being converted to equivalent airflow at full speed, i.e., 60 Hz. Then, uncertainty propagation of fan speed, airflow, fan head and fan power based on fan law conversion needs to be performed. Subsequently, rules for propagating uncertainties specified by ASHRAE Guideline 2 [1986] can be applied to define fan efficiency uncertainty.

### ***4.2.1 Uncertainty and error for input variables***

Fan head error is related to accuracy of installed DP sensors. According to manufacturers, installed DP sensors provide accuracy within  $\pm 1\%$  ( $\Delta H_i = 0.05 \text{ in. wg}$ ) for a selected pressure range of 0 to 5 inches of water.

Fan speed uncertainty needs to be included in the propagation of uncertainty for fan power. According to ANSI/ASHRAE Standard 51 [1999] this value can be estimated as

0.5% ( $U_{\omega} = 0.005$ ) since it can be easily obtained through VFD readings. Then, fan speed error can be defined as  $\Delta\omega_i = 0.005 \cdot 60\text{Hz} = 0.3\text{Hz}$ .

Fan power uncertainty is estimated to be within  $\pm 3\%$  ( $U_w = \pm 0.03$ ) full scale, according to the manufacturer. This value refers to reported accuracy for VFD's analog output connected to the BAS. Then, fan power error can be defined as Equation 4-1.

$$(4-1) \quad \Delta W_i = U_w \cdot W_{fan}$$

where  $W_{fan}$  refers to programmed fan power in kW in the VFD panel (see Table 2-1).

Airflow velocity measurement device uncertainty is estimated to be within  $\pm 2\%$  of reading ( $U_{velocity\ sensor} = 0.02$ ), according to the manufacturer.

Measured airflow velocity error is defined by Equation 4-2 through propagation of non-homothetic velocity distribution (i.e., RMSE% at 95% confidence for each case, according to Table 3-7-results for 3-P measurements) and  $U_{velocity\ sensor}$  uncertainties.

$$(4-2) \quad \Delta v_i = \pm v_i \cdot \sqrt{(2 \cdot RMSE\%)^2 + U_{velocity\ sensor}^2}$$

where  $v_i$  refers to measured average velocity in fpm by the 3-P method per minute  $i$ .

Length measurement error for width ( $L$ ) and depth ( $D$ ) of ductwork can be estimated at 1/8 inch each ( $\Delta L = \Delta D = 0.125\ \text{inch}$ ).

Area measurement error can be defined by Equation 4-3 [Hickman, 2004] as follows:

$$(4-3) \quad \Delta A = \pm \sqrt{\left| \frac{\partial A}{\partial L} \cdot \Delta L \right|^2 + \left| \frac{\partial A}{\partial D} \cdot \Delta D \right|^2}$$

where the derivatives for the area will depend on the duct shape, i.e., rectangular or oval duct sections.

Then, for rectangular ducts, the cross-sectional area is defined as follows:

$$(4-4) \quad A = L \cdot D$$

Then, the derivatives can be defined as follows:

$$(4-5) \quad \frac{\partial A}{\partial L} = D$$

$$(4-6) \quad \frac{\partial A}{\partial D} = L$$

For oval ducts, the cross-sectional area is defined as follows:

$$(4-7) \quad A = \frac{\pi \cdot D^2}{4} + D \cdot L - D^2$$

Then, the derivatives can be defined as follows:

$$(4-8) \quad \frac{\partial A}{\partial L} = D$$

$$(4-9) \quad \frac{\partial A}{\partial D} = \frac{\pi \cdot D}{2} + L - 2D$$

#### ***4.2.2 Error propagation***

In order to generate uncertainty bands for fan performance curves, error propagations for fan head, airflow, fan power and fan efficiency need to be performed. Described uncertainties and errors in Section 4.2.1 are fundamental for these uncertainty propagations.



Equivalent fan head error ( $\Delta H_e$ )

The analysis can be performed in the following manner, assuming a generic equation of the following form:

$$(4-10) \quad H_e = f(H_i, \omega_i)$$

where  $H_e$  refers to equivalent fan head in inches of water per minute  $i$ ,  $H_i$  refers to measured fan head in inches of water per minute  $i$ , and  $\omega_i$  refers to fan speed in Hz per minute  $i$ .

Then, according to Liu et al. [2005], equivalent fan head error can be described by Equation 4-11 based on fan law conversion by Equation 2-2 as follows:

$$(4-11) \quad \Delta H_e = \pm \sqrt{\left| \frac{\partial H_e}{\partial H_i} \cdot \Delta H_i \right|^2 + \left| \frac{\partial H_e}{\partial \omega_i} \cdot \Delta \omega_i \right|^2}$$

where the derivatives can be defined as follows:

$$(4-12) \quad \frac{\partial H_e}{\partial H_i} = \frac{(60\text{Hz})^2}{\omega_i^2}$$

$$(4-13) \quad \frac{\partial H_e}{\partial \omega_i} = \frac{-2 \cdot H_i \cdot (60\text{Hz})^2}{\omega_i^3}$$

Equivalent airflow error ( $\Delta Q_e$ )

The analysis can be performed in the following manner, assuming a generic equation of the following form:

$$(4-14) \quad Q_e = f(v_i, A, \omega_i)$$

where  $Q_e$  refers to equivalent airflow in cfm per minute  $i$ ,  $v_i$  refers to measured average velocity in fpm by 3-P method per minute  $i$ ,  $A$  refers to the cross-sectional area of

ductwork in ft<sup>2</sup> at the measurement location, and  $\omega_i$  refers to fan speed in Hz per minute  $i$ .

Then, based on Liu et al. [2005] deduction and fan law conversion by Equation 2-3, the equivalent airflow error can be defined by Equation 4-15 as follows:

$$(4-15) \quad \Delta Q_e = \pm \sqrt{\left| \frac{\partial Q_e}{\partial v_i} \cdot \Delta v_i \right|^2 + \left| \frac{\partial Q_e}{\partial A} \cdot \Delta A \right|^2 + \left| \frac{\partial Q_e}{\partial \omega_i} \cdot \Delta \omega_i \right|^2}$$

where the derivatives are defined as follows:

$$(4-16) \quad \frac{\partial Q_e}{\partial v_i} = \frac{A \cdot 60 \text{ Hz}}{\omega_i}$$

$$(4-17) \quad \frac{\partial Q_e}{\partial A} = \frac{v_i \cdot 60 \text{ Hz}}{\omega_i}$$

$$(4-18) \quad \frac{\partial Q_e}{\partial \omega_i} = \frac{-v_i \cdot A \cdot 60 \text{ Hz}}{\omega_i^2}$$

where  $A$  and  $\Delta A$  will depend on duct shape, i.e., oval for SF and rectangular for RF.

#### Equivalent fan power error ( $\Delta W_e$ )

The analysis can be performed in the following manner, assuming a generic equation of the following form:

$$(4-19) \quad W_e = f(W_i, \omega_i)$$

where  $W_e$  refers to equivalent fan power in kW at full fan speed (100%),  $W_i$  refers to measured fan power in kW per minute  $i$ , and  $\omega_i$  refers to fan speed in Hz per minute  $i$ .

Then, equivalent fan power can be obtained by applying Equation 4-20. Through this equation, it is possible to convert fan power at partial speeds to full speed, i.e., 60 Hz.

$$(4-20) \quad W_e = \frac{W_i}{\bar{\omega}^3}$$

where  $\bar{\omega}$  refers to the ratio of the partial speed (%) to the full speed, shown in Figure 2-3.

Then, equivalent airflow error is defined by Equation 4-21 based on Equation 4-20 as follows:

$$(4-21) \quad \Delta W_e = \pm \sqrt{\left| \frac{\partial W_e}{\partial W_i} \cdot \Delta W_i \right|^2 + \left| \frac{\partial W_e}{\partial \omega_i} \cdot \Delta \omega_i \right|^2}$$

where the derivatives can be defined as follows:

$$(4-22) \quad \frac{\partial W_e}{\partial W_i} = \frac{(60\text{Hz})^3}{\omega_i^3}$$

$$(4-23) \quad \frac{\partial W_e}{\partial \omega_i} = \frac{-3 \cdot W_i \cdot (60\text{Hz})^3}{\omega_i^4}$$

#### Fan efficiency error ( $\Delta\eta$ )

The analysis can be performed in the following manner, assuming a generic equation of the following form:

$$(4-24) \quad \eta = f(H_e, Q_e, W_e)$$

Then, Equation 2-1 shows that fan efficiency is obtained by multiplying and dividing measured variables. As a result, the propagation of uncertainties for multiplication and division need to be applied. To address these calculations, ASHRAE Guideline 2 [1986] shows that the propagation of uncertainties for two assumed independent variables ( $A$  and  $B$ ) with their respective errors ( $a$  and  $b$ ) can be generalized as follows:

For multiplication:  $(A \pm a) \cdot (B \pm b)$

$$(4-25) \quad U = \pm \sqrt{\left(\frac{a}{A}\right)^2 + \left(\frac{b}{B}\right)^2}$$

For division:  $(B \pm b) \div (A \pm a)$

$$(4-26) \quad U = \pm \frac{B}{A} \cdot \sqrt{\left(\frac{a}{A}\right)^2 + \left(\frac{b}{B}\right)^2}$$

Then, applying the general expression described by Equation 4-25 to variables in Equation 2-1, the uncertainty propagation for the product of the fan head and airflow can be defined as follows:

$$(4-27) \quad U_{Q_e \cdot H_e} = \pm \sqrt{\left(\frac{\Delta Q_e}{Q_e}\right)^2 + \left(\frac{\Delta H_e}{H_e}\right)^2}$$

Then, the error for the product of the fan head and airflow can be defined as follows:

$$(4-28) \quad \Delta(H_e \cdot Q_e) = \pm(H_e \cdot Q_e)U_{Q_e \cdot H_e} = \pm H_e \cdot Q_e \cdot \sqrt{\left(\frac{\Delta Q_e}{Q_e}\right)^2 + \left(\frac{\Delta H_e}{H_e}\right)^2}$$

Next, the uncertainty propagation for the division of  $H_e \cdot Q_e$  and  $W_e$  can be defined following Equation 4-26 as follows:

$$(4-29) \quad U_\eta = \pm \frac{H_e \cdot Q_e}{8507 \cdot W_e} \cdot \sqrt{\left(\frac{\Delta W_e}{W_e}\right)^2 + \left[\frac{\Delta(H_e \cdot Q_e)}{H_e \cdot Q_e}\right]^2}$$

Then, substituting  $\Delta(H_e \cdot Q_e)$  by Equation 4-28 in Equation 4-29 and simplifying, an expression for fan efficiency uncertainty can be defined by Equation 4-30 as follows:

$$(4-30) \quad U_\eta = \pm \frac{H_e \cdot Q_e}{8507 \cdot W_e} \cdot \sqrt{\left(\frac{\Delta W_e}{W_e}\right)^2 + \left(\frac{\Delta Q_e}{Q_e}\right)^2 + \left(\frac{\Delta H_e}{H_e}\right)^2}$$

Finally, the error propagation for fan efficiency can be defined by Equation 4-31 as follows:

$$(4-31) \quad \Delta\eta = \pm(\eta_i \cdot U_\eta)$$

where  $\eta_i$  refers to calculated fan efficiency per minute  $i$ .

### 4.3 Fan Performance Curves

Following the procedures introduced in Sections 4.1 and 4.2, in-situ fan performance curves were obtained for AHUs 5 and 9. Calibration results for AHU-6 are not presented because at the time of calibration, the BAS hardware of AHU-6 was damaged.

#### 4.3.1 AHU-5

Figures 4-3 and 4-4 show the obtained fan head and fan efficiency curves with uncertainty bands for 95% confidence for SF and RF of AHU-5.

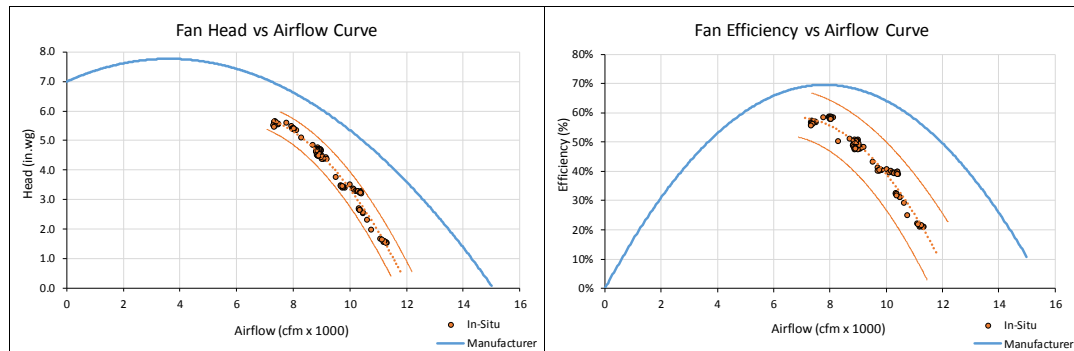


Figure 4-2: Fan performance curves for SF AHU-5.

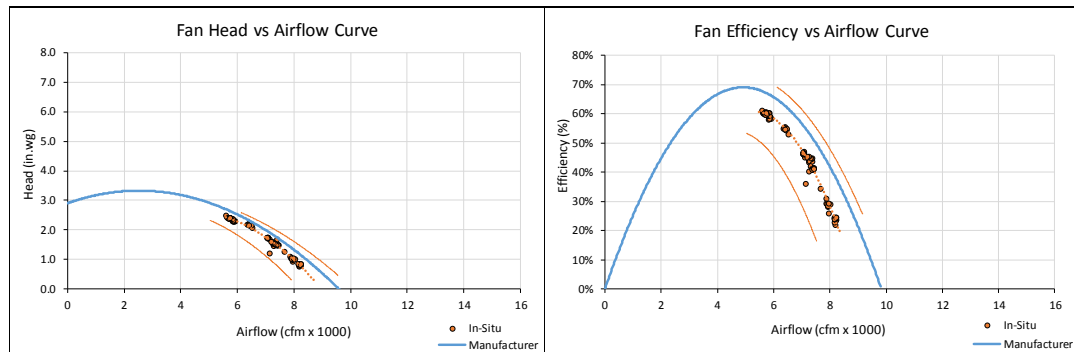


Figure 4-3: Fan performance curves for RF AHU-5.

Both figures show that measured fan curves are within ranges defined by the manufacturer's fan curves, but significant discrepancies exist. Both fans show to be operating below indicated performance by the manufacturer. Moreover, while the RF fan head curve indicates that the uncertainty bands are close to the manufacturer's curves, the SF curves show large discrepancies. Additionally, the fan efficiency curve for SF shows the calculated points to be more dispersed than RF. Nevertheless, SF uncertainty bands are narrower than those for RF, primarily because airflow measurement uncertainty is larger for RA measurements due to lower velocity ranges.

Moreover, the obtained in-situ performance curves suggest that the impact of system effects on SF is significantly larger than that obtained on RF. This is because a larger number of components for air distribution are installed on the SA side compared to components on the RA side. Additionally, the system effect impact involves distances from the inlet and outlet of fans to enclosure walls [Young et al., 2009]. Table 2-1 shows that SF is considerably larger in capacity, i.e., larger in size, than RF for all test AHUs. Thus, for test AHUs, where dimensions for SF and RF enclosures are the same, SF will have shorter separation to enclosure walls. Thus, the system effects impact due to wall separation will be larger for SF when compared to a smaller RF.

#### **4.3.2 AHU-9**

Figures 4-5 and 4-6 show the obtained fan head and fan efficiency curves with uncertainty bands for 95% confidence for SF and RF, respectively, of AHU-9.

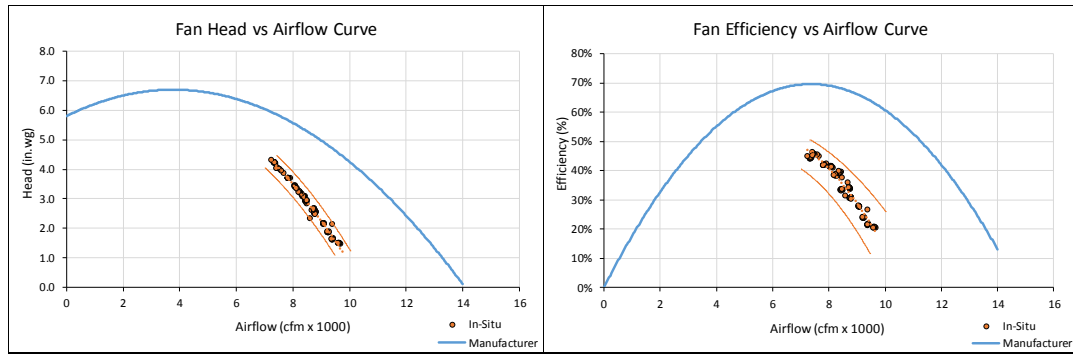


**Figure 4-4: Fan performance curves for SF AHU-9.**

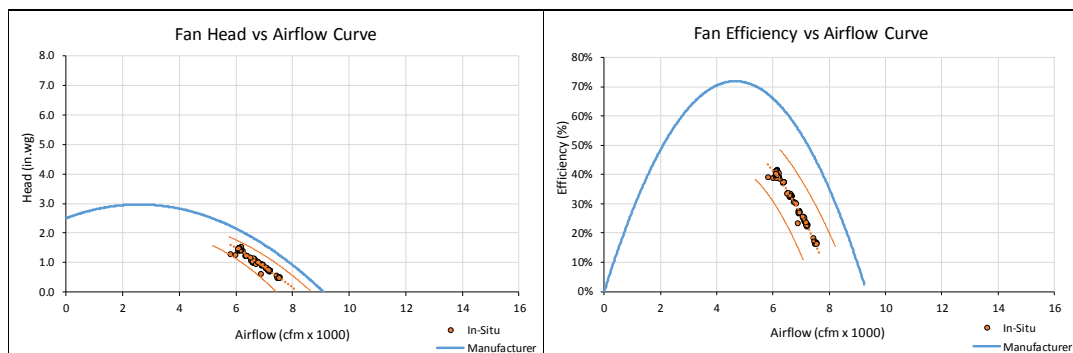


**Figure 4-5: Fan performance curves for RF AHU-9.**

Similar results to AHU-5 can be observed for the SF and RF performance curves. Both figures show that lower fan head and efficiency are obtained in-situ from fans when compared to manufacturer curves. Moreover, it is observed that SF presents larger discrepancies with manufacturer performance curves than RF. Additionally, like AHU-5, calculated fan efficiencies for SF show to be more dispersed than calculated efficiencies for RF.

Furthermore, the measured fan head and efficiency curve differences with manufacturer curves are significantly larger for AHU-9 in comparison to AHU-5. This suggests that fan inlet separation to enclosure walls is not the only factor lowering measured fan performance. As discussed in Chapter 3, close disturbances to the RA measurement plane

have created non-homothetic velocity distributions. The defined location factor in Section 3.3 can help account for the distance of disturbances to the measurement plane used for the TAB of the system. Table 3-8 shows that while the RA location factor for AHU-9 is 1.894 (highest value), it is 1.653 (lowest value) for AHU-5. More importantly, Figure 4-6 suggests that increasing the RA location factor will generate significant system effect impacts on measured in-situ RF performance curves. Following the same analysis, the measured SF performance curves at the outlet of fans showed to be less sensible to location factor.

#### **4.3.3 Summary**

Fan performance curves by manufacturers are commonly used in the field for TAB of VAV AHUs following industry standard suggestions. Nevertheless, system effects impacting both SF and RF performance will make the system operate with reduced performance. By comparing obtained in-situ fan performance curves to manufacturer curves, it is possible to support the validity of the results. Furthermore, actual operational ranges for both SF and RF are observed while accounting for system effects impact. This possibility allows for deciding whether modifications to system configuration are needed when commissioning to improve fan performance. Moreover, large discrepancies between in-situ and manufacturer performance curves are observed, and these discrepancies larger for SF than they are for RF. Nevertheless, observed uncertainty bands are narrower for SF performance curves when compared to those of RF.



## Chapter 5: Conclusions and Future Work

The overarching goal of this thesis work is to define a practical and reliable method for performing in-situ fan curve calibrations in VAV AHUs while ensuring compliance with ASHRAE Standard 111 [2008] accuracy requirements. The first objective addressed in this study was to complete airflow measurements for an extended time period using the traverse holes equipped for one-time TAB measurements. The second objective was to obtain in-situ fan performance curves while including predicted uncertainties.

Some key findings from testing the proposed airflow measurement method and calibration procedure for VAV AHUs are summarized below:

- It was observed that increasing sampling time up to 60 seconds helped to improve accuracy of 3-P measurements in both the SA and RA. No significant improvement was observed for sampling times beyond 60 seconds. In contrast, increasing sampling time beyond 60 seconds can indeed increase uncertainty, as results for AHU-9 illustrate.
- It was demonstrated that when airflow velocity is below 800 fpm, relative errors larger than 5% can be expected for 3-P average velocity. Extraordinarily large errors (20%) were found for 3-P average velocities below 400 fpm. Obtained results showed that errors above 5% were observed on RA measurements for fan speeds equal or lower than 50%. If obtained accuracy is above 5%, increasing number of sampling points can be applied as a strategy to achieve improvements of 2 to 3.5%. On the other hand, SA measurements were typically over 800 fpm and obtained relative errors were below 5% for every case. Then, obtained results

showed satisfactory accuracy ranges for 3-P measurements with no significant improvements when more sampling points were applied.

- A relationship between measurement location with respect to distance to disturbances and airflow measurement uncertainty was observed for SA. This relationship was defined by a location factor. Results showed that an increase in location factor can lead to an increase of uncertainty due to non-homothetic velocity profiles. The similarity of measurement conditions for RA in test AHUs did not allow for comparison of uncertainties. Future work should include performing uncertainty analysis for different measurement conditions on RA.
- It was verified that AFMS industry guidelines do not ensure obtaining airflow measurement uncertainties below 5%. By applying this guideline, based on the flow cross-sectional area, tested AHUs required 8 sampling points on both SA and RA ductwork. Results showed that 3-P measurements provided lower uncertainties than those obtained for 8-P, i.e., per AFMS guidelines. A tailored selection of sampling points proved to be effective in dealing with non-homothetic velocity profiles. This is because common AFMS guidelines do not account for in-situ installation conditions. Reducing sampling point density also reduces installation and maintenance costs of airflow measurement devices.
- The applied calibration procedure for VAV AHUs provided a wide enough range of operation for obtaining in-situ fan performance curves. Moreover, measured fan performance curves showed the actual operational range of SF and RF for in-situ conditions.

- The impact of system effects on fan performance was identified by comparing in-situ fan performance curves to manufacturer curves. Furthermore, results showed that under the impact of system effects, actual fan head curves for SF are similar to those of fans of smaller size. Thus, accounting for system effect impacts can help support improvement of system configuration during commissioning to regain fan performance.
- The impact of system effects was identified to be stronger on SF than RF. While close or overlapping in-situ and manufacturer fan head curves were observed for RF, curves for SF displayed significant discrepancies. This is because SF had a larger number of air distribution components and shorter separation to enclosure walls, which significantly reduced fan performance.

Based on these conclusions, some future tasks to complete and strengthen findings and contributions of this thesis work are as follows:

- Perform testing on fans of different sizes and brands to verify if reached conclusions are applicable to a broader variety of cases.
- Build a test bench to analyze the impact of specific location factor values on airflow measurement uncertainty for inlets and outlets of fan conditions.
- Quantify the impact of different types of disturbances to improve location factor definition by including impacts of measurement location and magnitude of disturbances.
- Design a prototype of DAQ with a built-in algorithm to perform, record and process traverse measurements to define the minimum number of sampling points required to comply with 5% of accuracy requirements.

## References

- [1] ASHRAE. 2008. ANSI/ASHRAE Standard 111-2008, *Practices for measurement, testing, adjusting, and balancing of building heating, ventilation, air-conditioning, and refrigeration systems*. Atlanta: American Society of Heating, Refrigerating and Air-Conditioning Engineers, Inc.
- [2] ASHRAE. 2013a. *ASHRAE Handbook-Fundamentals*, Chapter 3 and Chapter 36.
- [3] ASHRAE. 2013b. ANSI/ASHRAE/IES Standard 90.1-2013, *Energy Standard for Buildings Except Low-Rise Residential Buildings*. Atlanta: American Society of Heating, Refrigerating and Air-Conditioning Engineers, Inc.
- [4] ASHRAE. 2013c. ANSI/ASHRAE Standard 62.1-2013, *Ventilation for Acceptable Indoor Air Quality*. Atlanta: American Society of Heating, Refrigerating and Air-Conditioning Engineers, Inc.
- [5] ASHRAE. 2015. *ASHRAE Handbook-Applications*, Chapter 38.
- [6] ASHRAE. 2016. *ASHRAE Handbook HVAC Systems and Equipment*, Chapter 21.
- [7] ASHRAE. 2003. ASHRAE Guideline 16-2003, *Selecting Outdoor, Return, and Relief Dampers for Air-Side Economizer Systems*. Atlanta: American Society of Heating, Refrigerating and Air-Conditioning Engineers, Inc.
- [8] ASHRAE. 1999. ANSI/ASHRAE Standard 51-1999, *Laboratory Method of Testing Fans for Aerodynamic Performance Rating*. Atlanta: American Society of Heating, Refrigerating and Air-Conditioning Engineers, Inc.
- [9] ASHRAE. 1987. ASHRAE Guideline 2-1987, *Engineering Analysis of Experimental Data*. Atlanta: American Society of Heating, Refrigerating and Air-Conditioning Engineers, Inc.
- [10] ASTM. 2014. ASTM Standard D3464–96, *Standard Test Method for Average Velocity in a Duct Using a Thermal Anemometer*. ASTM International, West Conshohocken, PA.

- [11] Beck, B. T., Bardot, D. M., and Hosni, M. H. 2002. Uncertainty analysis of the experimental results investigating the effects of turbulence intensity on the performance of rotating vane anemometers/Discussion. *ASHRAE Transactions*, 108: 434.
- [12] Branesky, B. 2013. Energy Signature Development for Typical Faults at the Air Handling Unit-Level. M. S. thesis, Dept. of Aero. and Mech. Eng., Univ. of Oklahoma, Norman, OK.
- [13] Damiano, L. "Survey of Airflow Measurement Devices" (seminar presented at the National Environmental Balancing Bureau (NEBB) Annual Conference, Anaheim, CA: April 27, 2012).
- [14] Foltz, D. F. 1984. The systematic and random errors of portable airflow balancing instrumentation with various ventilation system fittings. *ASHRAE Transactions*, 90(2): 627-644.
- [15] GTx116-P+ Overview. EBTRON <http://ebtron.com/product/gtx116p/> [visited on August 31<sup>st</sup>, 2016]
- [16] Hickman, C. 2010. Determining the Effects of Duct Fittings on Volumetric Air Flow Measurements. M.S. thesis, Dept. Mech. and Nucl. Eng., Kansas St. Univ., Manhattan, KS.
- [17] Howell, R., and Sauer, H. 1989. Airflow Measurements at Coil Faces with Vane Anemometers-Experimental Results. *ASHRAE Transactions*, 95(2): 128-140.
- [18] Int-Hout, D. 2015. VAV Terminal Units: Looking Back, Ahead. *ASHRAE Journal*, October 2015: 40-49.
- [19] Krarti, M., Schroeder, C. C., Eric, J., and Brandemuehl, M. J. 2000. Experimental analysis of measurement and control techniques of outside air intake rates in VAV systems/Discussion. *ASHRAE Transactions*, 106: 39.
- [20] Liu, G. and Liu, M. Development of Simplified In-situ Fan Curve Measurement Method Using the Manufacturers Fan Curve. *Building and Environment* 48, 2012: 77-83.

- [21] Liu, M. 2002. Variable Speed Drive Volumetric Tracking (VSDVT) for Airflow Control in Variable Air Volume (VAV) Systems. *Journal of Solar Energy Engineering, Transactions of the ASME*, v 125, n 3: 318-323.
- [22] Liu, M., Liu, G., Joo, I., Song, L. and Wang, G. 2005. Development of In-situ Fan Curve Measurement for VAV AHU Systems. *Journal of Solar Energy Engineering, Transactions of the ASME*, v 127, n 2, May, 2005: 287-293.
- [23] McQuiston, F., Parker, J. and Spitler, J. 2005. *Heating, Ventilation, and Air Conditioning*, 6<sup>th</sup> ed. New York: John Wiley & Sons, Inc.
- [24] Morris, D. M., Beck, B. T., and Hosni, M. H. 2001. Experimental determination of the effects of turbulence intensity on the performance of rotating vane anemometers. *ASHRAE Transactions*, 107: 215.
- [25] Rivas Prieto, A., Elizondo, J., Song, L. and Wang, G. 2016a. Uncertainty Studies of Airflow Measurements in Non-Ideal Conditions in Variable Air Volume Air Handling Units. *ASHRAE Annual Conference*, St. Louis, MO
- [26] Rivas Prieto, A., Thomas, W., Song, L. and Wang, G. 2016b. In-Situ Fan Curve Calibration for Virtual Airflow Sensor Implementation in VAV Systems. *ASHRAE Transactions*, accepted.
- [27] Schroeder, C. C., Krarti, M., and Brandemuehl, M. J. 2000. Error analysis of measurement and control techniques of outside air intake rates in VAV systems. *ASHRAE Transactions*, 106: 26.
- [28] Schwenk, D. M. 1998. Air flow measurement accuracy. US Army Corps of Engineers, Construction Engineering Research Laboratories (USACERL). Champaign, IL.
- [29] Taylor, S. 2014. Return fans in VAV systems. *ASHRAE Journal*, October 2014: 54-58.
- [30] Thomas, W. 2014. Simulation and Experimentation for Air Handling Unit Supply Air Temperature Optimal Control. M. S. thesis, Dept. of Aero. and Mech. Eng., Univ. of Oklahoma, Norman, OK.

- [31] TSI Inc. 2012. Performing a Duct Traverse. [https://www.youtube.com/watch?v=cNxIY\\_c7gM0](https://www.youtube.com/watch?v=cNxIY_c7gM0) [visited on September 7<sup>th</sup>, 2016]
- [32] Wang, G. and Liu, M. 2005. Development of Power-head based fan airflow station. *Proceedings of International Conference for Enhanced Building Operations 2005*, Pittsburgh, PA.
- [33] Wang, G. and Liu, M. 2007. Development of Motor Power Based Fan Airflow Station, *Proceedings of Energy Sustainability 2007*, Long Beach, CA.
- [34] Wang, G., Liu, M. and Claridge, D. 2010. Demonstration of an Energy Meter Using a Pump Flow Station. *ASHRAE Transactions, v 116 Part 2*.
- [35] Wang, G., Song, L. and Park, S. 2012. Estimation of Induction Motor Efficiency under Variable Frequencies. *AEI/ASHRAE EXPO*. Omaha, NE.
- [36] Wildi, T. 2000. *Electrical Machines, Drives, and Power Systems*. Prentice Hall, Upper Saddle River, NJ.
- [37] Young, M., Darvennes, C. and Idem, S. 2008. Aerodynamic Performance and System Effects of Propeller Fans. *HVAC&R Research, Vol. 15, March 2009*: 231-254.
- [38] Young, M. N., Darvennes, C., and Idem, S. 2009. Aerodynamic Performance and System Effects of Propeller Fans (RP-1223). *HVAC&R Research 15 (2)*: 231-254.
- [39] Yuill D. P., Redmann, N. and Liu, M. 2003. Development of Fan Airflow station for Airflow Control in VAV systems. *Proceedings of International Solar Energy Conference 2003*: 4-9.

## **Appendix A: Abbreviations**

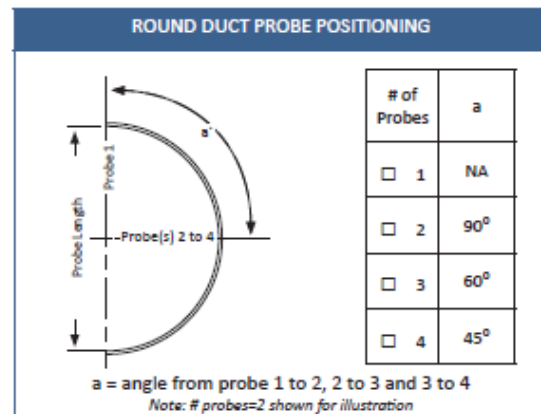
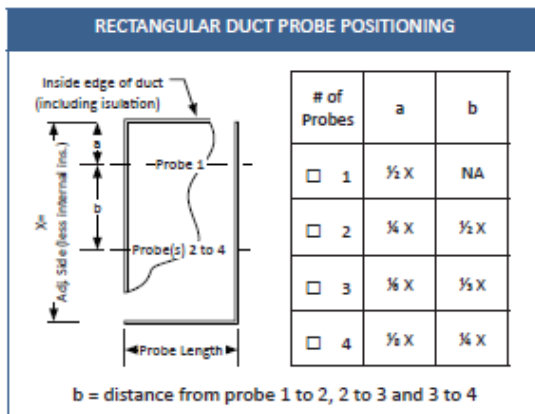
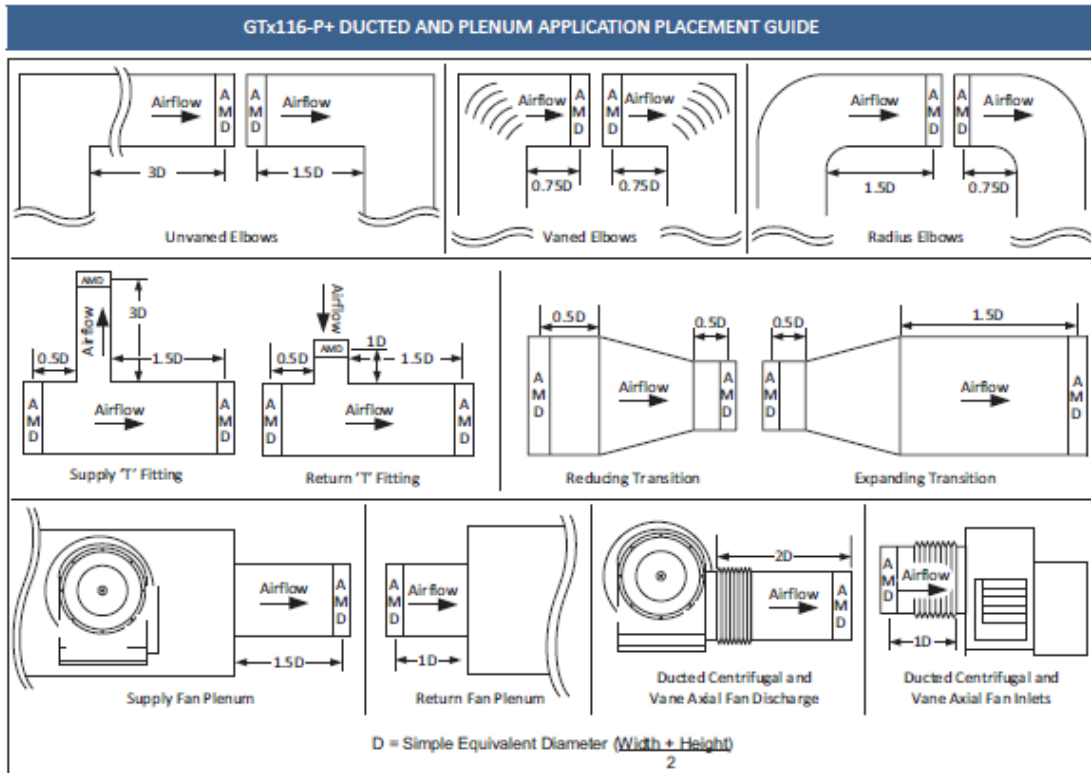
ASHRAE	American Society of Heating, Refrigerating and Air Conditioning Engineers
VAV	Variable Air Volume
CAV	Constant Air Volume
AHU	Air Handling Unit
HVAC	Heating, Ventilation and Air Conditioning
IAQ	Indoor Air Quality
TAB	Testing, Adjusting and Balancing
VFD	Variable Frequency Drive
DP	Differential Pressure
BAS	Building Automated System
DAQ	Data Acquisition Device
SA	Supply Airflow
RA	Return Airflow
OA	Outdoor Air
RMSE	Root Mean Square Error
RMSE%	Relative Error
SF	Supply Fan



RF	Return Fan
3-P	3-Point Measurement
5-P	5-Point Measurement
9-P	9-Point Measurement
AFMS	Air Flow Measurement Station
VAFM	Virtual Airflow Meter
$\bar{\omega}$	Fan Speed Ratio
$H$	Fan Head (in inches of water)
$H_i$	Measured Fan Head under Partial Fan Speed
$H_e$	Equivalent Fan Head by Fan Laws
$Q$	Fan Airflow Rate (in cubic feet per minute)
$Q_i$	Measured Fan Airflow Rate under Partial Fan Speed
$Q_e$	Equivalent Fan Airflow Rate by Fan Laws
$W$	Fan Power (in kilowatt)
$W_i$	Measured Fan Power under Partial Fan Speed
$W_e$	Equivalent Fan Power by Fan Laws
$\eta$	Overall Fan Efficiency

## Appendix B: AFMS Industry Guidelines

Area (sq.ft.) [sq.m]	Sensor Nodes	Area (sq.ft.) [sq.m]	Sensor Nodes
≤ 0.5 [0.046]	1	> 4 & ≤ 8 [0.743]	8
> 0.5 & ≤ 1 [0.092]	2	> 8 & ≤ 12 [1.11]	12
> 1 & ≤ 2 [0.185]	4	> 12 & ≤ 14 [1.30]	14
> 2 & ≤ 4 [0.371]	6	> 14 [1.30]	16



**NOTES:**

The GTx116-P+ sensor density will typically result in an installed accuracy of ±3% of reading or better over the entire calibrated range of airflow rates when locations meet or exceed EBTRON's suggested guidelines. Installed accuracy is the combined uncertainty of the measuring device and the sampling uncertainty that results from having a finite number of sensor nodes in a velocity profile created by duct disturbances up and downstream of the measurement location.

Source: EBTRON, 2016